Quaternary Geochronology 92 (2026) 101726

Contents lists available at ScienceDirect

Quaternary Geochronology

journal homepage: www.elsevier.com/locate/quageo

Luminescence chronology of the Velika Vrbica loess-palaeosol sequence (Wallachian Basin): Evaluating quartz and K-feldspar signals from MIS 5 to the Holocene

Zoran M. Perić [a,*], Cathal S. Ryan [b], Milica G. Bosnić [c], Petar Krsmanović [c], Warren Thompson [d,e], Helena Alexanderson [a], Slobodan B. Marković [c,f,g,h]

[a] Department of Geology, Lund University, Sölvegatan 12, SE-223 62, Lund, Sweden
[b] Irish Climate Analysis and Research Units, Department of Geography, Maynooth University, Maynooth, Ireland
[c] Department of Geography, Tourism and Hotel Management, Faculty of Sciences, University of Novi Sad, Trg Dositeja Obradovića 3, 21000, Novi Sad, Serbia
[d] The National Museum of Denmark, Frederiksholms Kanal, Prinsens Palæ, DK-1200, København K, Denmark
[e] Technical University of Denmark, Risø Campus, Frederiksborgvej 399 - Building 201, 4000, Roskilde, Denmark
[f] Division of Geochronology and Environmental Isotopes, Institute of Physics - Centre for Science and Education, Silesian University of Technology, Gliwice, Poland
[g] Serbian Academy of Sciences and Arts, Kneza Mihaila 35, 11000, Belgrade, Serbia
[h] University of Montenegro, Cetinjska 2, 81000, Podgorica, Montenegro

ARTICLE INFO

Keywords:
Quartz OSL dating
K-feldspar pIRIR$_{290}$ signal
Linear modulated OSL (LM-OSL)
Bayesian age-depth modelling
Loess

ABSTRACT

The Velika Vrbica loess-palaeosol sequence, situated on the south-western bank of the Danube River in north-eastern Serbia, represents one of the key Quaternary records in the lower Danube basin, covering the MIS 5-MIS 1 period. Previous investigations of the upper 500 cm established a high-resolution chronology and revealed unexpected patterns of dust accumulation during interstadial phases. In this study, we extend the analysis to the full ~12 m thickness of the sequence, spanning from Marine Isotope Stage (MIS) 5 to the Holocene, with emphasis on refining the geochronological framework and testing the performance of different luminescence signals. A comprehensive set of quartz optically stimulated luminescence (OSL) and K-feldspar post-infrared infrared stimulated luminescence (pIRIR$_{290}$) ages, complemented by linear modulated OSL (LM-OSL) analyses, provides a robust chronology. Bayesian age-depth modelling constrains the timing of key stratigraphic units, including the S1 palaeosol (MIS 5), the overlying L1 loess (MIS 4–2) with its interstadial palaeosol (L1SS1), and the Holocene soil (S0). Quartz and K-feldspar ages display systematic differences: younger deposits show feldspar overestimation consistent with incomplete bleaching, whereas older horizons (MIS 5–4) yield excellent agreement between the two signals. LM-OSL results confirm that the fast component dominates most of the profile, supporting the reliability of equivalent dose determinations across multiple stratigraphic units. The resulting chronology demonstrates that the Velika Vrbica site preserves a continuous record of loess accumulation and pedogenesis over the last ~130 ka. These findings not only refine the temporal framework for south-eastern European loess but also provide an important evaluation of the applicability and limitations of quartz and K-feldspar luminescence signals in establishing long-term chronologies.

1. Introduction

Loess-palaeosol sequences (LPS) are among the most important terrestrial archives of Quaternary climate and environmental change. Their alternating loess layers and palaeosols document the rhythm of glacial-interglacial cycles, preserving information on dust fluxes, pedogenesis, and environmental conditions (e.g. Buggle et al., 2013; Marković et al., 2015; Perić et al., 2019; Stevens et al., 2011). Detailed stratigraphic and geochronological analyses of LPS not only enable the reconstruction of regional palaeoclimate histories but also provide the chronological framework necessary for evaluating environmental processes in a global context (Marković et al., 2015). South-eastern Europe, and particularly the Wallachian Basin, hosts some of the most extensive and continuous loess deposits worldwide (e.g. Jordanova et al., 2022).

* Corresponding author.
E-mail address: zoran.peric@geol.lu.se (Z.M. Perić).

https://doi.org/10.1016/j.quageo.2026.101726
Received 17 October 2025; Received in revised form 9 January 2026; Accepted 15 January 2026
Available online 16 January 2026

The Velika Vrbica LPS, located on the south-western bank of the Danube River near the Iron Gates Gorge, marks the westernmost margin of this basin. Owing to its position along a major fluvial corridor and within a climatically sensitive region, it preserves an exceptional record of Quaternary environmental dynamics. Recent research on the upper 500 cm of the Velika Vrbica profile has provided new insights into dust accumulation patterns and sedimentation dynamics, supported by high-resolution optically stimulated luminescence (OSL) dating (Perić et al., 2025a). These results suggest that regional dust deposition was not restricted to glacial maxima but also intensified during interstadial phases, challenging established paradigms of loess accumulation. However, the chronology of the deeper part of the sequence, which encompasses Marine Isotope Stage (MIS) 5 to MIS 4, has not yet been systematically investigated. The present study extends the chronological framework to the complete Velika Vrbica LPS. By applying a combination of quartz OSL and K-feldspar post-IR IRSL (pIRIR) dating, complemented by linear modulated OSL (LM-OSL) analyses, we aim to establish a robust age-depth model and evaluate the reliability of different luminescence signals across multiple glacial-interglacial cycles. This integrated approach enables us to assess potential issues of incomplete bleaching, fading, and signal stability, while also testing the agreement between quartz and K-feldspar ages over both young and old deposits. Through this geochronological framework, the Velika Vrbica LPS provides new constraints on sediment accumulation rates and environmental change in the lower Danube basin from MIS 5 to the Holocene. In doing so, this study advances our understanding of loess chronologies in south-eastern Europe and contributes to broader discussions on the temporal limits and reliability of luminescence dating in Eurasian loess records.

2. Site setting and description

The Velika Vrbica LPS is situated in north-eastern Serbia (latitude 44°35′1.70″N, longitude 22°43′15.97″E), approximately 10 km east of the city of Kladovo and ~20 km downstream of the Iron Gate gorge (Fig. 1). Positioned near the Danube River, the site rises ~20 m above its south-western bank, marking the westernmost boundary of the Wallachian Basin. The LPS has a total thickness of ~12 m and consists of a series of loess layers and fossil soils underlain by a fluvial terrace (Fig. 2) (Krsmanović et al., 2025; Perić et al., 2025a). The base of the exposed section comprises the uppermost 45 cm of the L2 loess unit. This sediment is porous and contains numerous carbonate concretions and dark humic infiltrations. Its contact with the overlying pedocomplex is irregular and strongly reworked by bioturbation. The S1 pedocomplex itself is 2.3 m thick and is internally differentiated into several horizons: a basal reddish AB layer with weak angular blocky structure, overlain by two humus-rich, granular Ah horizons (Ah2 and Ah1), and culminating in a weakly developed A horizon marking the transition to glacial conditions. Overlying S1 is the L1 unit, a 7.85 m thick loess package documenting the last glacial cycle. It is subdivided into three subunits. The basal L1LL2 subunit (8.60–5.50 m) consists of porous, pale loess with minimal alteration. Above it lies the L1SS1 subunit (5.50–4.20 m), a 1.30 m thick, weakly developed palaeosol of interstadial age (MIS 3), identified by its darker colour and granular structure. The uppermost L1LL1 subunit (4.20–0.75 m) consists of pale yellow, unaltered loess and contains a 1.1 m thick bed of aeolian sand in its upper part. According to the established age model (Perić et al., 2025a), its lower part belongs to MIS 3, while the bulk accumulated during MIS 2. The top ~10 cm represents deposition at the transition to the Holocene. The sequence is capped by the modern soil (S0), a 75 cm thick horizon recording Holocene pedogenesis. In summary, the Velika Vrbica LPS provides a near-continuous record of environmental change from beyond MIS 5 to the present, capturing evidence of interglacial and interstadial soil development alongside episodes of intense loess deposition.

3. Methods

3.1. Sample preparation and facilities

With the exception of the two lowermost samples (1040 and 1105 cm) used for luminescence dating, samples were collected at ~50 cm intervals from the Velika Vrbica profile. Stainless steel cylinders (20 cm

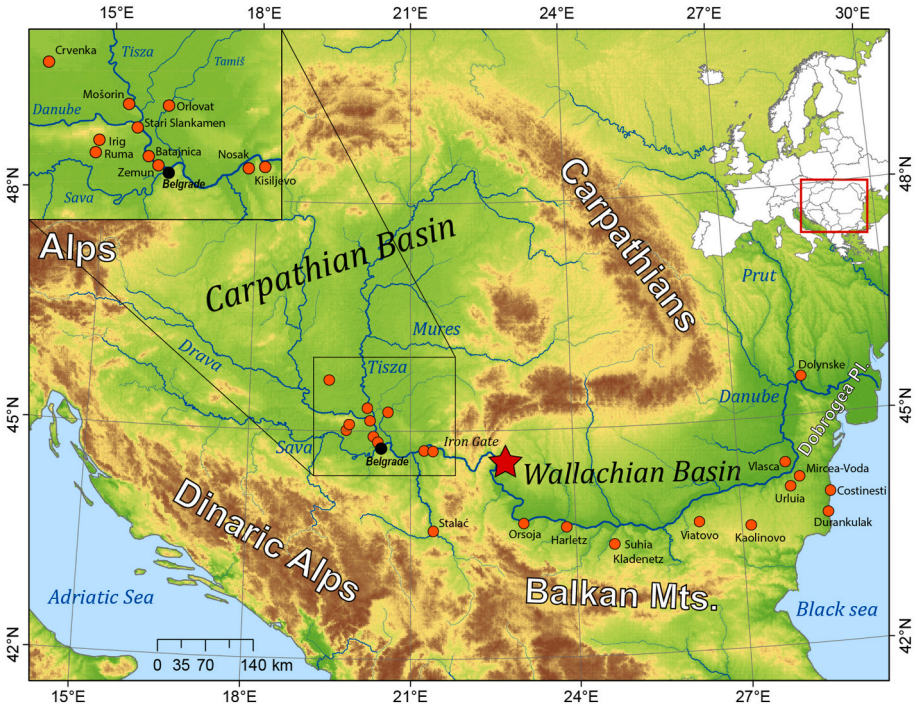

Fig. 1. Map of the middle and lower Danube Basin showing the position of the Velika Vrbica LPS (red star) and other important LPSs in the region (red circles) (adopted from Perić et al., 2025).

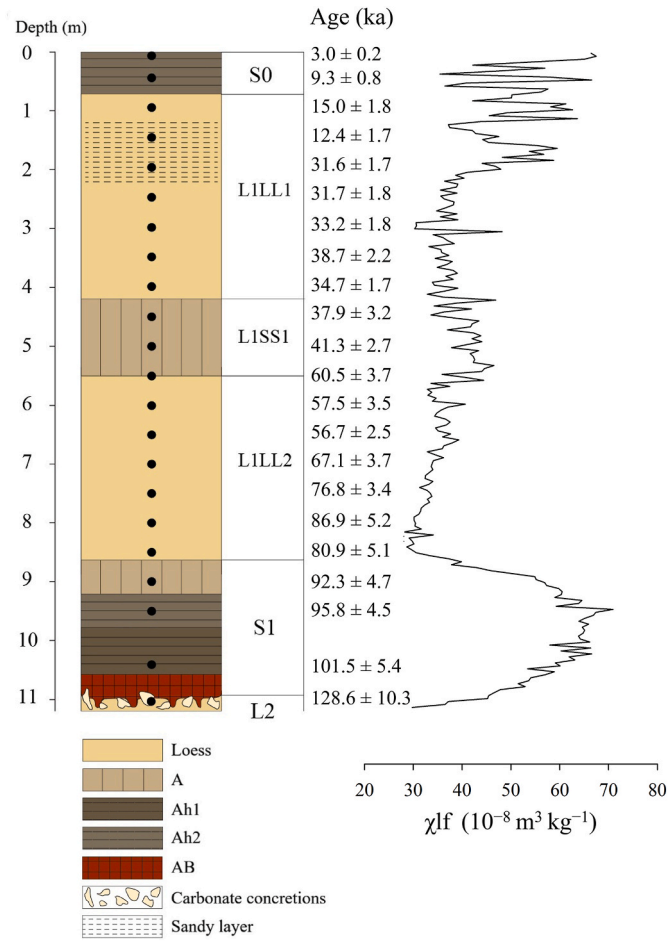

Fig. 2. Lithological column for the Velika Vrbica LPS, with OSL sample locations (solid black circles) and preferred ages (adopted from Perić et al., 2025). Also shown are the measured MS values. Horizon designations: A (initial pedogenesis), Ah1 (upper humic), Ah2 (lower humic), and AB (transitional horizon).

long, 5 cm in diameter) were hammered horizontally into freshly cleaned sections of the exposure to minimize light contamination. In the laboratory (Lund Luminescence Laboratory, Lund University, Sweden), all preparation steps were performed under subdued red light. The outer ~2 cm of material from each tube, which may have been exposed to daylight, was separated and used for water content determination and dose rate assessment. The inner portion of the sample was wet-sieved to obtain the 63–90 μm fraction. Quartz and K-feldspar were then isolated through a series of chemical and density separation steps. Carbonates and organic matter were removed with 10 % HCl (60 min) and 10 % H_2O_2 (60 min), respectively. Heavy-liquid separation using sodium heteropolytungstate (density 2.62 g cm^{-3}; LST "Fastfloat") was applied to separate quartz (density >2.62 g cm^{-3}) from K-feldspar (density <2.62 g cm^{-3}). The quartz fraction was further etched with 40 % HF for 90 min to eliminate residual feldspar and to clean the grain surfaces, followed by a 10 % HCl wash (120 min) to dissolve any fluoride precipitates. For K-feldspar, a second density separation step (LST at 2.58 g cm^{-3}) was used to isolate K-feldspar from Na-feldspar. The K-feldspar fraction was then etched with 10 % HF for 20 min and subsequently treated with 10 % HCl for 40 min. Prepared grains were mounted on stainless steel discs using silicone oil: 8 mm aliquots for quartz OSL and 2 mm aliquots for K-feldspar IRSL. Luminescence measurements were performed using Risø TL/OSL DA-20 readers (Bøtter-Jensen et al., 2003), equipped with blue light-emitting diodes (470 nm, ~80 mW cm^{-2}) and infrared diodes (870 nm, ~135 mW cm^{-2}). Irradiations were carried out with a $^{90}Sr/^{90}Y$ beta source calibrated against Risø calibration quartz (batch 123; Hansen et al., 2015). Quartz OSL emissions were detected through a 7.5 mm Hoya U-340 UV filter, while K-feldspar pIRIR signals were recorded using a combination of Corning 7–59 and Schott BG-39 filters. Data reduction and analysis were undertaken using the Risø TL/OSL software package (Duller, 2015).

3.2. Dose rate measurements

Dose rates were determined using two different methodological approaches. For samples 22181-22182, high-resolution gamma spectrometry (HRGS) was performed at the Nordic Laboratory for Luminescence Research, Technical University of Denmark (DTU). For samples 22183-22193, dose rates were acquired using the μDose system at the Lund Luminescence Laboratory, following established protocols (Kolb et al., 2022; Tudyka et al., 2023). For the HRGS measurements, approximately 100 g of sediment from each sample was oven-dried, ground to <20 μm, and heated at 450 °C for 24 h to remove organic matter. The prepared material was mixed with wax and cast into disc-shaped containers designed to retain ^{222}Rn. Samples were sealed and stored for over 21 days to allow secular equilibrium between ^{226}Ra and ^{222}Rn to be established. Measurements of ^{238}U, ^{232}Th, and ^{40}K concentrations were conducted over a 24-h period using a high-resolution gamma spectrometer calibrated according to Murray et al. (2005). Radionuclide concentrations were converted to dry dose rates using the conversion factors of Guérin et al. (2011) for quartz and of Adamiec and Aitken (1998) for K-feldspar.

For the μDose measurements, sediment samples were dried at 105 °C for 24 h and ground to <20 μm. Approximately 3 g of material from each sample was placed in a 70 mm diameter holder. Activity concentrations of ^{238}U, ^{232}Th, and ^{40}K were measured over >24 h, and dry dose rates were calculated using the same conversion factors as for the HRGS method.

Measured water content was very low for all samples, likely due to prolonged aerial exposure of the profile prior to sampling. As these values were not considered representative of long-term burial conditions, a constant water content of 15 ± 5 % was adopted, as outlined by Perić et al. (2025a).

Alpha and beta attenuation corrections were applied using the factors of Brennan et al. (1991) and Guérin et al. (2012), respectively, for quartz grains. For K-feldspar grains, the alpha attenuation factors of Bell (1980) and the beta factors of Guérin et al. (2012) were used. An internal dose rate of 0.10 ± 0.05 Gy/ka, derived from U and Th was assumed for the K-feldspar samples (Mejdahl, 1987; Zhao and Li, 2005). In addition, K and Rb concentrations of 12.5 ± 0.5 % and 400 ± 100 ppm, respectively, were adopted for the K-feldspar grains (Huntley et al., 2001; Huntley and Baril, 1997).

The cosmic dose rate was calculated based on sample depth, density, altitude, latitude, and longitude, with an associated uncertainty of 10 % (Prescott and Hutton, 1994). Final dose rates and corresponding luminescence ages were computed using the DRAC dose rate and age calculator (Durcan et al., 2015). All measured radionuclide concentrations are presented in Table 1.

3.3. Equivalent dose and quartz saturation measurements

To ensure consistency and comparability across the entire sequence, for the equivalent dose (D_e) measurements of the quartz grains, we applied the same experimental settings as those established in the study by Perić et al. (2025a), where the upper 500 cm of the Velika Vrbica profile was dated. Feldspar contamination was evaluated using the IR depletion test (IR/B ratio). All the quartz samples in this study showed values < 10 % and were measured using the SAR protocol (Murray and Wintle, 2000, 2003). For SAR measurements, quartz grains were run with preheat and cut-heat temperatures of 240 °C and 200 °C, respectively. The OSL signals were recorded with a channel resolution of 0.08 s

Table 1
Summary of sample codes, depth information, stratigraphic units, radionuclide activities, total dose rates ($\dot{D}$), weighted mean D_e values, OSL and $pIRIR_{100,\ 290}$ ages for the Velika Vrbica samples. n represents the number of accepted aliquots.

Sample id	Depth (cm)	Unit	^{238}U (ppm)	^{232}Th (ppm)	^{40}K (%)	n	OSL D_e (Gy)	Total $\dot{D}$ (Gy/ka)	OSL age (ka)	n	pIRIR D_e	Total $\dot{D}$ (Gy/ka)	pIRIR age (ka)
22172	10	S0	*1.8 ± 0.3*	*10.5 ± 0.2*	*1.5 ± 0.1*	*31*	*7.6 ± 04*	*2.5 ± 0.1*	*3.0 ± 0.2*	6	16.3 ± 0.3	3.1 ± 0.2	5.2 ± 0.3
22173	50	S0	*2.0 ± 0.8*	*9.4 ± 0.2*	*1.3 ± 0.1*	*20*	*21.1 ± 1.2*	*2.3 ± 0.1*	*9.3 ± 0.8*	6	38.7 ± 0.7	2.9 ± 0.2	13.3 ± 0.9
22174	100	L1LL1	*1.7 ± 0.3*	*6.8 ± 0.2*	*1.1 ± 0.0*	*17*	*28.8 ± 3.2*	*1.9 ± 0.1*	*15.0 ± 1.8*	6	55.8 ± 0.8	2.5 ± 0.1	22.4 ± 1.3
22175	150	L1LL1	*1.7 ± 0.8*	*7.4 ± 0.2*	*1.1 ± 0.1*	*28*	*23.8 ± 2.7*	*1.9 ± 0.1*	*12.4 ± 1.7*	6	56.3 ± 0.7	2.5 ± 0.2	22.5 ± 1.6
22176	200	L1LL1	*2.4 ± 0.6*	*6.3 ± 0.2*	*1.0 ± 0.0*	*14*	*61.0 ± 3.1*	*1.9 ± 0.1*	*32.2 ± 2.6*	6	77.0.8 ± 1	2.5 ± 0.2	31.0 ± 2.2
22177	250	L1LL1	*2.6 ± 0.9*	*9.4 ± 0.3*	*1.3 ± 0.1*	*22*	*82.6 ± 4.9*	*2.4 ± 0.2*	*34.2 ± 3.1*	6	92.4 ± 1.2	3.1 ± 0.2	29.6 ± 2.2
22178	300	L1LL1	*2.5 ± 0.9*	*10.4 ± 0.2*	*1.5 ± 0.1*	*21*	*83.2 ± 5.0*	*2.6 ± 0.2*	*32.2 ± 2.8*	6	113.3 ± 1.3	3.3 ± 0.2	34.3 ± 2.4
22179	350	L1LL1	*2.6 ± 0.8*	*10.3 ± 0.2*	*1.4 ± 0.1*	*14*	*93.7 ± 8.1*	*2.5 ± 0.1*	*37.4 ± 3.9*	6	128.0 ± 1.5	3.2 ± 0.2	39.6 ± 2.7
22180	400	L1LL1	*3.0 ± 0.8*	*10.8 ± 0.2*	*1.5 ± 0.1*	*17*	*96.1 ± 3.3*	*2.7 ± 0.2*	*35.2 ± 2.4*	6	118.9 ± 1.6	3.5 ± 0.2	34.1 ± 2.4
22181	450	L1SS1	*1.7 ± 0.9*	*11.8 ± 0.3*	*1.7 ± 0.1*	*23*	*101.7 ± 5.6*	*2.7 ± 0.2*	*37.9 ± 3.2*	6	143.8 ± 1.9	3.4 ± 0.2	42.8 ± 3.0
22182	500	L1SS1	*3.1 ± 0.6*	*12.9 ± 0.2*	*1.8 ± 0.0*	*24*	*128.1 ± 6.1*	*3.1 ± 0.1*	*41.3 ± 2.7*	5	177.6 ± 6.1	3.9 ± 0.2	45.7 ± 3.1
22183	550	L1SS1	2.1 ± 0.6	17.9 ± 2.0	1.6 ± 0.1	22	182.3 ± 3.6	3.0 ± 0.2	60.5 ± 3.7	6	209.2 ± 2.8	3.9 ± 0.3	54.3 ± 4.0
22184	600	L1LL2	1.9 ± 0.6	16.6 ± 2.0	1.7 ± 0.1	45	167.7 ± 2.3	2.9 ± 0.2	57.5 ± 3.5	6	182.2 ± 3.0	3.7 ± 0.3	49.1 ± 3.6
22185	650	L1LL2	3.1 ± 0.5	10.5 ± 1.7	1.7 ± 0.1	47	156.8 ± 2.2	2.8 ± 0.2	55.6 ± 3.2	6	209.3 ± 5.9	3.6 ± 0.2	58.5 ± 4.1
22186	700	L1LL2	2.2 ± 0.4	12.1 ± 1.2	1.7 ± 0.1	12	182.8 ± 4.7	2.7 ± 0.1	67.1 ± 3.7	6	260.4 ± 3.9	3.5 ± 0.2	75.4 ± 4.7
22187	750	L1LL2	2.3 ± 0.5	10.8 ± 1.5	1.6 ± 0.1	11	202.2 ± 4.9	2.6 ± 0.1	77.2 ± 4.6	6	254.1 ± 4.2	3.3 ± 0.2	76.3 ± 5.0
22188	800	L1LL2	1.5 ± 0.5	12.7 ± 1.7	1.7 ± 0.1	33	228.1 ± 3.9	2.6 ± 0.2	86.9 ± 5.2	6	314.2 ± 4.7	3.3 ± 0.2	94.8 ± 6.5
22189	850	L1LL2	1.5 ± 0.5	13.0 ± 1.7	1.8 ± 0.1	11	217.6 ± 5.7	2.7 ± 0.2	80.9 ± 5.1	6	334.9 ± 5.0	3.4 ± 0.2	99.0 ± 6.7
22190	900	S1	1.7 ± 0.5	13.4 ± 1.7	1.6 ± 0.1	7	235.4 ± 11	2.6 ± 0.1	90.1 ± 6.6	6	315.2 ± 7.9	3.3 ± 0.2	94.7 ± 6.8
22191	950	S1	0.5 ± 0.4	18.1 ± 1.3	1.7 ± 0.1	10	259.9 ± 9.1	2.8 ± 0.1	94.3 ± 5.8	6	340.9 ± 7.3	3.5 ± 0.2	97.7 ± 7.2
22192	1040	S1	0.2 ± 0.5	17.4 ± 1.7	1.6 ± 0.1	9	247.6 ± 9.6	2.5 ± 0.1	98.8 ± 6.9	6	334.9 ± 8.0	3.2 ± 0.2	104.7 ± 8.4
22193	1105	L2	0.9 ± 0.5	11.8 ± 1.6	1.2 ± 0.1	8	238.3 ± 8.3	2.0 ± 0.1	119.1 ± 8.9	6	338.1 ± 10.3	2.6 ± 0.2	128.6 ± 10.3

Note: The values in italic are adopted from Perić et al. (2025a).

per channel. The net signal was derived from the first two recorded channels (channels 11–12; 0–0.16 s), and the background was estimated from channels 13–14 (0.32–0.48 s). A test dose of ~10 % of the natural dose was used for sensitivity correction, and each SAR cycle concluded with a 280 °C cleanout, for 40 s. The rejection of aliquots was based on the criteria of Murray and Wintle (2003), whereby measurements exceeding tolerance limits for recycling ratio (±10 %) or recuperation (>5 %) were excluded from D_e calculation. This led to the rejection of 17 % of all measured quartz aliquots. The OSL signal was best fitted using either a single saturating exponential or an exponential + linear function.

To evaluate the degree of signal saturation for the newly analysed quartz samples (22183–22193), we followed the same approach as described by Perić et al. (2025a). The sensitivity-corrected natural luminescence signal (L_n/T_n) for each sample was compared to the laboratory-saturated signal (L_x/T_x) obtained after administering a dose of approximately 4000 Gy, with the latter determined from the dose-response curve of sample 22181 (25.34 ± 0.77). The ratio $(L_n/T_n)/(L_x/T_x)$ therefore reflects the proportion of the natural signal relative to laboratory saturation. For this group of samples, the calculated ratios vary between 0.13 ± 0.00 (sample 22184) and 0.18 ± 0.01 (sample 22183), yielding an average value of 0.15 ± 0.01 (Table S1). These results show that all measured signals are far below the 86 % saturation threshold (equivalent to 2 × D_0; Wintle and Murray, 2006), indicating that none of the corresponding OSL ages are affected by dose saturation and can therefore be regarded as reliable.

D_e determinations on K-feldspar grains were carried out using the post-IR IRSL SAR protocol at 290 °C ($pIRIR_{290}$; Buylaert et al., 2012; Thiel et al., 2011). Aliquots were first preheated at 320 °C for 60 s and subsequently exposed twice to infrared (IR) diode stimulation for 200 s. The first IR stimulation was performed at 100 °C, providing the IRSL signal, while the second stimulation at 290 °C yielded the post-IR IRSL signal ($pIRIR_{100,290}$), which was used for D_e calculation. A test dose corresponding to approximately 30 % of the expected natural signal was administered and measured following the same procedure (Yi et al., 2015). The rationale for using 100 °C as the initial stimulation temperature is addressed in a subsequent section. Each SAR cycle concluded with a 200 s IR illumination at 325 °C to minimize signal recuperation. Measurements were performed sequentially on individual aliquots, with six aliquots analysed per sample. Quality control involved standard performance checks, including recycling ratios and recuperation tests. Based on these criteria, no K-feldspar aliquots were rejected. The pIRIR signals were extracted from the first 2 s of stimulation, after subtracting a background signal obtained from the final 50 s. The dose–response curve constructed from the $pIRIR_{290}$ signal was fitted using a single saturating exponential function. Representative dose response curves for the quartz and K-feldspar samples, together with the decay curves of natural signals and regenerated signals are presented in Fig. 3A and B. The blue-light stimulated OSL signal from quartz displays a rapid decay within the first second of stimulation (inset, Fig. 3A), which is characteristic of well-bleached quartz dominated by the fast OSL component. The natural and regenerative decay curves are indistinguishable, indicating excellent reproducibility of the signal and effective sensitivity correction during measurement. The dose response curves for quartz were best described by either a single saturating exponential or an exponential-plus-linear function, consistent with the expected behavior of quartz OSL signals approaching saturation at higher doses. The mean recycling ratio for samples 22183-22193 was 0.99 ± 0.01, and the recuperation was 0.07 ± 0.01 % (n = 215). These values fall well within acceptable limits, confirming that the applied SAR protocol effectively compensates for sensitivity changes and that the OSL signal is stable and reproducible. Similarly, the IR-stimulated $pIRIR_{290}$ signal from K-feldspar samples (22172–22193) also exhibits a rapid initial decay (inset, Fig. 3B) during the first 2 s of stimulations, and the natural and regenerative decay curves overlap closely, indicating reliable signal reproducibility. The corresponding dose response curves were best fitted with a single saturating exponential function. The mean recycling ratio was 0.99 ± 0.00, while the mean recuperation was 1.42 ± 0.10 % (n = 132), both of which suggest that the measurement protocol provides robust correction for sensitivity changes and that the residual signal contribution is minimal.

Overdispersion (OD) was quantified for both quartz OSL and $pIRIR_{290}$ D_e distributions to assess the scatter beyond analytical uncertainties, which can reflect incomplete bleaching, microdosimetric heterogeneity, or post-depositional mixing. For quartz, OD values ranged from ~14 % to 68 % (Table S2), with the highest values in the youngest and most recently reworked units (S0, upper L1LL1). In contrast, $pIRIR_{290}$ D_e values exhibited substantially lower OD, typically between 2 % and 29 %. This pattern confirms the $pIRIR_{290}$ signal's superior resetting during transport and its greater homogeneity in well-

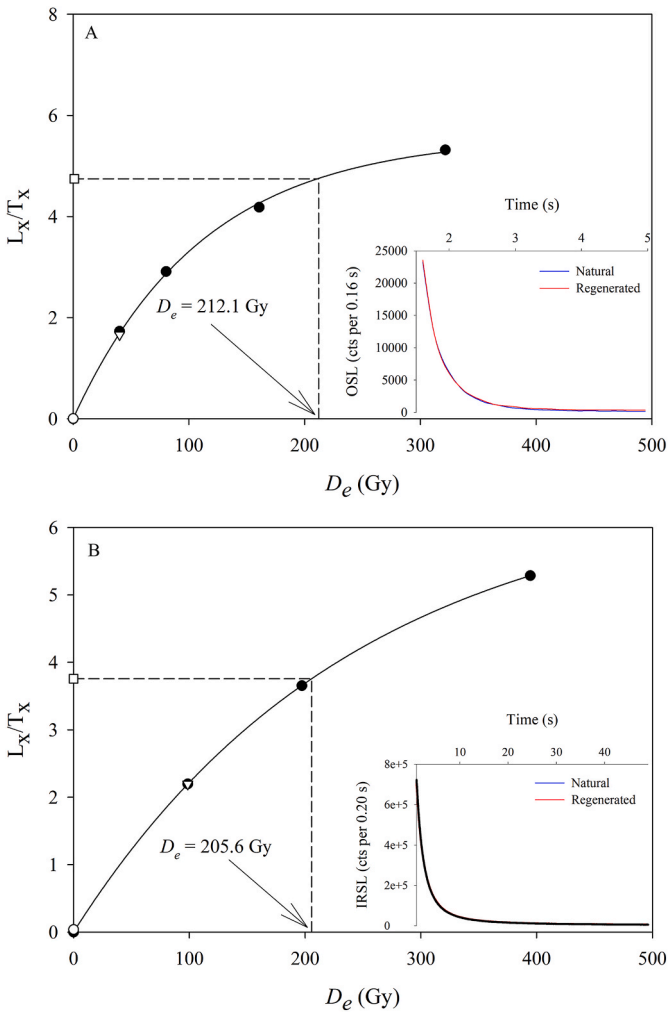

Fig. 3. Sensitivity-corrected luminescence dose-response curves for (A) quartz OSL and (B) K-feldspar $pIRIR_{100,\ 290}$ sample 22184. Natural signals (open squares) and corresponding equivalent doses (dashed lines) are shown, with zero-dose responses (open circles) and recycling points (open inverted triangles). Insets display typical decay curves of natural signals (blue) compared with regenerated signals (red) induced by β doses ~ equal to the equivalent dose.

bleached, older deposits. Despite the higher scatter in quartz D_e values, the close agreement between quartz and feldspar ages in units older than ~50 ka indicates that the observed OD primarily reflects natural depositional variability rather than systematic bias, supporting the reliability of the derived chronology.

3.4. Linear modulated OSL measurements

Linear Modulated OSL (LM-OSL) measurements were conducted on the natural quartz signal only, without analysing any regenerated doses. The samples were measured for 1000 s at 125 °C while linearly increasing the power of the blue LEDs from 0 to 78 mW cm^{-2}. To determine the background, one additional blank aliquot was prepared, and the photon count rate was measured following the same protocol used for the quartz grains. This approach was chosen to characterize LM-OSL response across the entire loess profile, specifically, to assess changes in trap-component contributions with depth and to explore potential shifts in sediment provenance. Laboratory bleaching and regeneration are known to alter trap occupancies and re-weight component contributions, potentially introducing artefacts and complicating interpretation; focusing on the natural signal ensures the LM-OSL curves reflect the pristine, in-situ trap populations. This strategy is supported in the literature: Bailey et al. (2001) emphasized the importance of preserving natural signal characteristics when interpreting OSL component structure. Laboratory treatments like heating and bleaching cause complex charge transfer between different traps (electron and hole centres). The decision to analyse only the natural LM-OSL signal is also supported by provenance studies, such as Sawakuchi et al. (2018), which demonstrate that the intrinsic luminescence characteristics of quartz are a direct fingerprint of sediment source and transport history. Since our primary aim was to track provenance shifts with depth in the loess profile, we prioritized the pristine, unaltered natural signal to avoid the potential for laboratory dosing and bleaching to re-weight component contributions and obscure the original sedimentary signature.

The LM-OSL measurements were analysed by deconvolving the composite signal into its constituent components using the fit_LMCurve function of the R Luminescence package (Kreutzer et al., 2012). The data was fitted according to the equation of Bulur (1996):

$$L(t) = \sum A_i b_i\ (t / \mathrm{P}) \exp\left(b_i t^2 / 2\mathrm{P}\right) \quad (1)$$

where $L(t)$ represents the luminescence intensity as a function of time t, A_i is the amplitude, b_i is the detrapping probability (which is proportional to the photoionisation cross-section σ_i and the maximum light intensity I_0; $b_i = \sigma_i . I_0$), and P is the total stimulation time.

The quality of each fit was quantitatively assessed using a coefficient of determination (pseudo-R^2), calculated as:

$$R^2_{pseudo} = 1 - \frac{SS_{res}}{SS_{tot}} \quad (2)$$

where SS_{res} is the difference between the LM-OSL curve and the fitted one, while SS_{tot} represents the variance of the observed signal around its mean.

Aliquots were subject to a two-tiered rejection criteria to ensure the robustness of the subsequent component analysis.

- Poor Model Fit: Aliquots were rejected if the fitted model failed to provide a satisfactory description of the measured data, indicated by a pseudo-R^2 value below 0.85. We adopt a criterion of pseudo-$R^2 \geq$ 0.85, similar to general usage of goodness-of-fit thresholds in OSL deconvolution studies (Kitis et al., 2011; Kitis and Pagonis, 2008) for discussion of LM-OSL vs CW-OSL deconvolution and component stability. A low pseudo-R^2 signifies that a significant portion of the variance in the data remains unexplained by the model, rendering the extracted physical parameters (e.g., photoionisation cross-sections, initial electron concentrations) statistically unreliable.
- Model Complexity and Representativeness: The optimal number of components (*k*) for each aliquot was determined by identifying the model that minimized the Bayesian Information Criterion (BIC; Peng et al., 2014) while also achieving a high goodness-of-fit (pseudo-$R^2 \geq$ 0.85). This approach aligns with established recommendations for OSL decay-curve decomposition, where statistical criteria help avoid under- or over-fitting of component models (Adamiec, 2005). This number varied between samples, reflecting natural differences in mineralogical composition and trap population densities. For a given sample, the mode of the distribution of *k* was identified. Aliquots from that sample, which required a model of significantly lower complexity (e.g., *k* = 2 for a sample where the mode was *k* = 4), were rejected. This inconsistency indicated that the fitting procedure failed to resolve the full complement of luminescence components present in the majority of aliquots, likely due to poor signal-to-noise ratio or an unstable measurement, thereby yielding a non-representative and oversimplified picture of the sample's trap system. Conversely, aliquots requiring a more complex model (e.g., *k* = 5 for a sample where *k* = 4 was typical) were scrutinized for

overfitting but were accepted if the additional component was physically plausible and improved the goodness-of-fit.

Aliquots meeting both criteria: a high-quality fit (pseudo-$R^2 > 0.85$) and a model complexity consistent with the sample's characteristic trap structure were retained for final analysis. While the pseudo-R^2 statistic provides a clear measure of the variance explained by the model, we note that alternative metrics, such as the Figure of Merit (Balian and Eddy, 1977), may offer enhanced sensitivity to variations in fitting performance. For the purposes of this study, which focuses on the overall component structure and its stratigraphic consistency, the pseudo-R^2 criterion was deemed sufficient and is consistent with common practice in luminescence component analysis.

Based on these requirements, only sample 22178 was omitted from the analysis. The LM-OSL measurement for this sample failed, most likely because the amount of quartz grains was too small to yield a reliable result.

3.5. Age-depth modelling and magnetic susceptibility measurements

To establish a robust and continuous chronology for the Velika Vrbica loess-palaeosol sequence, we integrated the OSL and $pIRIR_{290}$ ages using an age-depth model. This approach addresses the inherent challenges of luminescence dating, where individual ages can exhibit significant scatter or reversals due to incomplete bleaching, reworking, or analytical error. The model was constructed within the Bayesian framework of rbacon (Blaauw and Christen, 2011), which incorporates age uncertainties and enforces stratigraphic superposition to interpolate between dated levels. We used a section thickness of 20 cm (thick), a resolution of 5 cm (d.by), and 200,000 iterations (ssize) to ensure model convergence. The final chronology provides a more reliable estimate of sediment accumulation rates and enables direct comparison with other regional palaeoclimate records.

The magnetic susceptibility (χ) analyses followed the procedure described in Perić et al. (2025a). A total of 221 samples were collected at 5 cm intervals, homogenized, and packed into non-magnetic 7 cm^3 cubes. Measurements were performed in the Palaeomagnetic Laboratory, Lund University, Sweden, using an AGICO Kappabridge MFK2 with a field strength of 200 A/m and a frequency of 976 Hz. Data were processed with SAFYR7 software.

4. Results

4.1. Radionuclide concentrations

The activity concentrations of ^{238}U, ^{232}Th, and ^{40}K show systematic and stratigraphically coherent variations that delineate the contrasting processes of loess deposition and palaeosol formation. It is important to note that the methodological approach differed with depth: samples from 10 to 500 cm (22172-22182) were measured by HRGS, while samples from 550 to 1105 cm (22183-22193) were measured using the uDose system. This results in generally larger associated uncertainties for the deeper samples, particularly for ^{232}Th, which must be considered in the interpretation. The modern soil (S0) exhibits elevated and stable concentrations of ^{232}Th (9.38–10.47 ppm) and ^{40}K (1.25–1.46 %), consistent with ongoing pedogenic enrichment of these immobile elements (Buggle et al., 2008). Uranium-238 concentrations are moderate (1.83–1.95 ppm) but are characterized by a high analytical uncertainty in this unit (Fig. 4).

The upper loess unit (L1LL1) displays a clear geochemical evolution with depth. The top of the unit (100–200 cm) is marked by the lowest concentrations of ^{232}Th (6.31–7.36 ppm) and ^{40}K (0.99–1.13 %) in the entire HRGS-measured profile, representing the unaltered, mineralogical signature of rapidly deposited glacial dust (e.g. Liu, 1985). With increasing depth, a pronounced upward-decreasing trend is observed, with ^{232}Th and ^{40}K values rising to 10.80 ppm and 1.54 %, respectively,

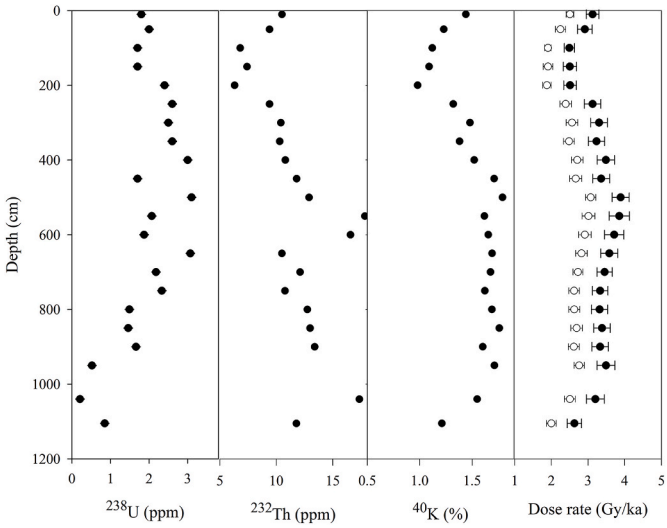

Fig. 4. Summary of the measured radionuclide concentrations for ^{238}U, ^{232}Th, and ^{40}K. Also presented are the total measured environmental dose rates for quartz (open circles) and K-feldspar (full circles) samples. The error bars represent one standard error.

at 400 cm. Conversely, ^{238}U shows an opposing trend, increasing from 1.66 ppm to 3.00 ppm at the base of the unit. This geochemical convergence towards palaeosol-like values at ~400 cm suggests a weakly developed pedocomplex, indicating a less harsh climatic interval prior to the main phase of loess accumulation.

The L1SS1 palaeosol displays a significant peak in radionuclide concentrations associated with pedogenesis (e.g. Buggle et al., 2008). The unit shows a strong enrichment in ^{232}Th, reaching a maximum of 12.87 ppm (HRGS) at 500 cm. The first sample measured by the uDose system (22183 at 550 cm) indicates a further significant increase to 17.85 ppm, though with a substantially larger uncertainty (±1.99 ppm). Potassium-40 concentrations also peak in this unit (1.81 %). These maxima confirm that L1SS1 represents a period of intense chemical weathering and clay mineral formation during a past interglacial period (Buggle et al., 2008; Gallet et al., 1996). The L1LL2 unit exhibits unexpectedly high and variable concentrations of ^{232}Th (10.49–16.57 ppm) and ^{40}K (1.62–1.76 %) for a loess layer, with characteristically high uncertainties from the uDose measurements. These values are atypical for primary, unweathered loess and closely resemble those found in paleosols. This anomalous signal, combined with the high variability, suggests that this unit is not a primary loess deposit but has likely been significantly altered by post-depositional processes, such as weathering and pedogenic overprinting, or represents a reworked sediment layer (Kemp, 2001).

The S1 palaeosol, displays the most extreme geochemical differentiation, indicative of highly mature soil development (Buggle et al., 2008; Gallet et al., 1996). It is characterized by sustained enrichment of ^{232}Th (11.78–18.11 ppm) and the strongest depletion of ^{238}U (0.21–0.85 ppm) in the entire sequence. The near-complete leaching of soluble ^{238}U under warm, humid, and well-drained conditions is a classic signature of intense pedogenesis (e.g. Buggle et al., 2008). A sharp decline in ^{40}K to 1.21 % at the top of the L2 unit (1105 cm) likely marks the lower boundary of the weathering front and the transition into unweathered parent material.

Here, we have to note that the increased uncertainties for ^{232}Th in samples below 500 cm (uDose data) preclude direct quantitative comparison of absolute concentrations with the overlying HRGS data. However, the robust stratigraphic patterns of enrichment and depletion remain clearly visible and are consistent with the established pedostratigraphy. The key interpretations are based on these relative trends within and between units rather than on absolute values alone.

4.2. Thermal stability and dose recovery

The thermal stability of the $pIRIR_{290}$ signal was evaluated by measuring the dependence of D_e on the first IR stimulation temperature. Fifteen aliquots of a representative K-feldspar sample (22172) were measured with temperatures ranging from 50 to 250 °C in 50 °C steps. As illustrated in Fig. 5A, the D_e values show a pronounced dependence on preheat temperature. A small but well-defined plateau, indicating thermally stable signal behavior, is evident between 100 and 150 °C. At higher temperatures, the D_e values noticeably increases, suggesting the influence of unstable charge populations. This is corroborated by the rapid depletion of the $pIRIR_{290}$ signal itself (Fig. 5B), which decreases exponentially with temperature, falling to 23 % of its 100 °C value by 200 °C and being virtually eliminated (0.7 %) at 250 °C. Therefore, a first IR stimulation temperature of 100 °C was selected for all samples, as it maximizes signal intensity while ensuring D_e stability.

To evaluate the reliability of the $pIRIR_{100,290}$ protocol, a dose recovery test was employed. Incremental beta doses of approximately 50, 100, 200, and 400 Gy were administered to the natural sample (22172) without any prior bleaching, meaning the added doses were superimposed onto the existing natural dose. The identical $pIRIR_{100,290}$ SAR protocol used for D_e determination was then applied to these dosed aliquots. The test dose was set to 30 % of the total dose, and three aliquots were measured per dose point.

The measured dose from the protocol represents the total dose (natural + administered). To isolate the signal from the added beta dose, the highest measured natural D_e of the sample was subtracted from each measured value. The ratio of the given dose to this calculated recovered dose was then determined. The results yielded mean recovery ratios of 0.98 ± 0.01, 0.88 ± 0.02, 0.91 ± 0.02, and 0.92 ± 0.02 for the 50, 100, 200, and 400 Gy doses, respectively (Fig. 6). It is noticeable that the measured dose slightly underestimates the given one at 100 Gy, however, however, when considering the associated uncertainty, it still lies within the 10 % acceptance limits. This small underestimation is likely due to a minor imperfection in the sensitivity correction for that specific test dose size, but this should not be regarded as a major concern (e.g. Buylaert et al., 2012). The protocol demonstrated excellent accuracy at 50 Gy and consistent, acceptable recovery (0.91–0.92) at higher doses, proving its overall reliability. Therefore, we consider the chosen $pIRIR_{100,290}$ SAR protocol as robust.

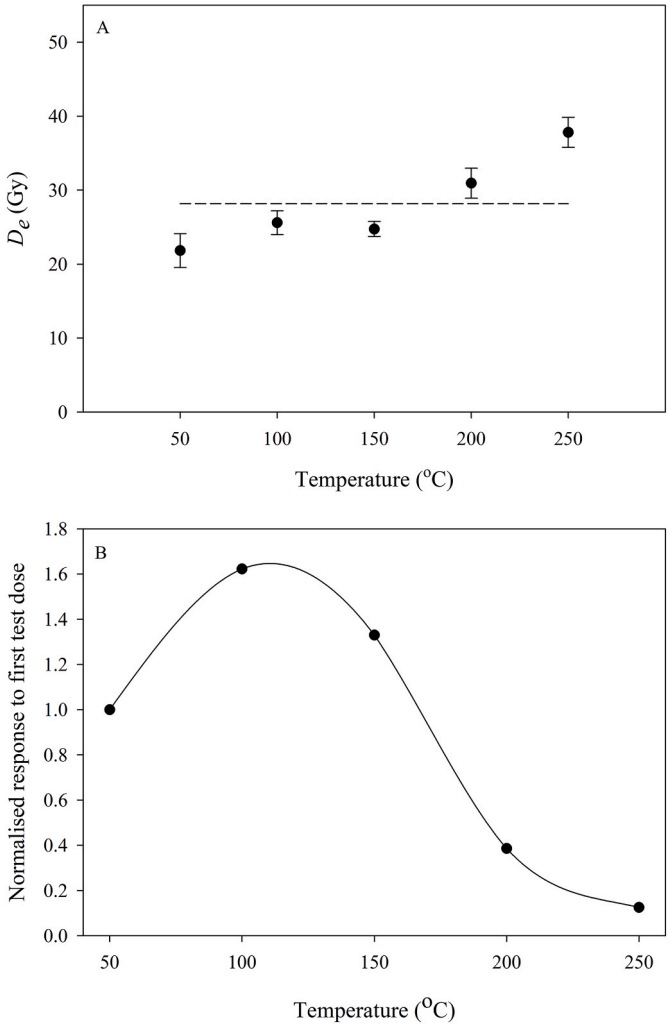

Fig. 5. A) Results of the first IR stimulation plateau test for sample 22172. Error bars denote one standard error. The dashed line indicates the mean D_e value calculated across all five temperature points. (B) $pIRIR_{290}$ response to the initial (natural) test dose plotted against the first stimulation temperature for sample 22172. Data are normalized to the natural $pIRIR_{290}$ test-dose response following the first IR stimulation at 50 °C. Three aliquots were analysed per temperature point.

4.3. Residual dose measurements

The assessment of the unbleachable residual dose is critical for the accuracy of $pIRIR_{290}$ ages. In this study, the residual dose of 7.9 ± 0.3 Gy was determined by bleaching aliquots under natural sunlight in Lund, Sweden (placed in a window), during the months of June–July for a period of 30 days. The residual dose was measured in the same manner as for the D_e determination (3 aliquots) and subsequently subtracted from the K-feldspar D_e values prior to age calculation. This approach is methodologically superior to laboratory solar simulators as it replicates the full spectral composition of natural daylight, thereby providing a more accurate estimate of the truly bleachable component of the signal (e.g. Kars et al., 2014). However, a fundamental uncertainty is introduced by the geographical and seasonal context of the bleaching experiment: it was conducted under the long, bright summer days of southern Sweden, while the samples originate from the Velika Vrbica site in Serbia's Wallachian Basin. This means that while the spectrum was natural, the duration and high intensity (a single high-latitude geographic location/optimal season) represent a best-case scenario, it may not fully capture the integrated bleaching history of the sediment in its depositional environment, which likely experienced shorter exposure

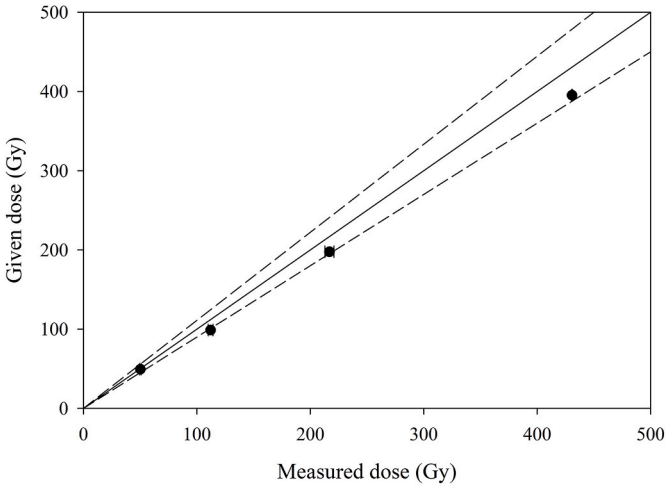

Fig. 6. Dose recovery results for four Velika Vrbica samples. Given irradiation doses were 50, 100, 200, and 400 Gy, with test doses set to ~30 % of the administered dose. Three aliquots were measured per sample. The solid line marks the ideal 1:1 dose recovery ratio, while the dashed lines indicate a ±10 % deviation from this line. The error bars represent one standard error.

times, lower solar angles, and potentially less optimal conditions (e.g., turbid water, shaded settings). Therefore, while our residual dose correction is based on a robust empirical experiment and is certainly applicable, we acknowledge that it might slightly underestimate the true residual dose that would be found in a naturally bleached sample. Consequently, for the few samples in the upper sequence where incomplete bleaching is suspected (based on quartz-feldspar age comparisons), the $pIRIR_{290}$ ages should be considered maximum limiting ages. For the well-bleached, older deposits (>50 ka) that form the core of this study, the impact of any such minor underestimation is negligible relative to the large palaeodoses and associated uncertainties. This pattern is also well-documented in other loess-palaeosol sequences across Eurasia (e.g. Buylaert et al., 2011; Li and Li, 2011; Thiel et al., 2011). For these horizons, quartz ages were therefore adopted as the preferred chronology.

In addition to residual dose considerations, the reliability of the pIRIR signal also depends on the possibility of anomalous fading. In our case, the K-feldspar ages show close agreement with their quartz OSL counterparts, leaving little reason to suspect significant fading in the $pIRIR_{290}$ signal. Indeed, as highlighted by Buylaert et al. (2012), even when fading is detectable, it may largely reflect artefacts of the measurement procedure rather than true signal instability. This reduces the dependence of the method on fading correction models, which inherently rely on untestable assumptions. In our dataset, the application of fading corrections would not improve the accuracy, consistency, or stratigraphic coherence of the age results. We therefore refrain from implementing any fading correction, considering the close agreement between quartz and K-feldspar ages to provide strong empirical evidence for the robustness of our chronology.

4.4. LM OSL characteristics

To allow for meaningful comparison between samples with different absolute detrapping probabilities, the photoionisation cross-section (σ) for each component is expressed relative to the fast component of the same sample (Relative Cross-section, Table 2). The absolute σ values are provided for completeness but should be interpreted with the understanding that they are dependent on the specific experimental stimulation parameters (Bulur, 1996). The key parameters for interpretation are the relative cross-section and the percentage contribution of each component.

Representative LM-OSL curves for S0 (10 cm), L1LL1 (150 and 200 cm) and L1LL2 (650 cm) are presented in Fig. 7 and Table 2, while the complete set for all measured samples is shown in Fig. S1 and Table S3.

The LM OSL signals from the studied loess-palaeosol sequence are dominated by the fast component throughout most of the profile. In most samples, the fast component contributes more than 85 % of the total signal, and frequently exceeds 90–95 %. The corresponding pseudo-R^2 values are consistently high (0.92–0.98), confirming the robustness of the component fitting and overall reliability of the decompositions. Clear differences are observed between stratigraphic units. In the modern soil (S0), the fast component remains dominant (>85 %), but medium and slow components reach up to 13 %, suggesting minor mixing of signal contributions. The loess units (L1LL1 and L1LL2) generally show strong fast components (>90 %) and limited medium/slow contributions, confirming that unaltered loess deposits provide particularly clean OSL signals. However, specific horizons deviate from this trend: at 150 cm (L1LL1) the fast component contributes only 32 % while the medium component dominates at 55 %; and at 200 cm (a sandy layer within L1LL1) the fast component drops to 56 % with a medium component contribution of 27 % and multiple slow components present. In L1LL2, the majority of samples again show fast contributions >90 %, but at 650 cm the fast component decreases to 58 % with the medium component contributing 39 %. The palaeosols (L1SS1 and S1) show strong and stable fast component signals (>88–99 %), with medium and slow components rarely exceeding 10 %. This suggests that pedogenically altered horizons still retain luminescence properties dominated by the fast component, making them suitable for dating. Fast component b-values are generally consistent across the sequence (3.5–4.5), reflecting stable luminescence kinetics. Deviations occur at 150 cm (0.72) and 200 cm (6.05), which coincide with the horizons exhibiting anomalous component distributions.

In summary, the LM-OSL results confirm that the loess-palaeosol sequence yields high-quality luminescence signals dominated by the fast component, supporting their suitability for equivalent dose determination. The few exceptions (notably at 150, 200, and 650 cm), most likely correspond to stratigraphic transitions, provenance change or sedimentological disturbances (e.g., sandy intercalations).

4.5. Magnetic susceptibility

The magnetic susceptibility (χlf) record at the Velika Vrbica LPS

Table 2
LM-OSL component fitting results for four representative Velika Vrbica samples. Shown are the sample ID, stratigraphic unit, depth, number of measured aliquots (n), identified components, detrapping probability (b), photoionisation cross-section (σ), relative cross-section, component contribution (%), and pseudo-R^2 values. Relative cross-sections are normalized to the fast component of each sample. Absolute σ values are influenced by experimental stimulation parameters (Bulur, 1996) The relative values and component contributions (%) are the primary focus for interpretation.

Sample id	Unit	Depth (cm)	n	Component	Detrapping probability (b)	Photoionisation cross-section (σ)	Relative Cross-section	Component contribution (%)	pseudo-R^2
22172	S0	10	3	Fast	3.85 ± 0.00004	2.3^{-17}	1	87.3	0.965
				Medium	0.03 ± 0.005	8.8^{-18}	0.2	11.4	
				Slow1	0.0005 ± 0.00006	2.7^{-22}	0.00	1.3	
22175	L1LL1	150	4	Fast	0.72 ± 0.18	4.0^{-18}	1	32.4	0.982
				Medium	0.1 ± 0.008	5.9^{-19}	0.1	54.5	
				Slow1	0.03 ± 0.004	1.5^{-19}	0.04	10.9	
				Slow2	0.002 ± 0.0003	1.3^{-20}	0.003	2.2	
22176	L1LL1	200	6	Fast	6.05 ± 0.96	3.6^{-17}	1	55.8	0.927
				Medium	2 ± 2.239	1.2^{-17}	0.3	27.4	
				Slow1	0.2 ± 0.1	1.2^{-18}	0.03	7.9	
				Slow2	0.06 ± 0.03	3.7^{-19}	0.01	7.0	
				Slow3	0.015 ± 0.012	8.8^{-20}	0.003	1.3	
				Slow4	0.0016 ± 0.0009	8.9^{-21}	0.0002	0.7	
22185	L1LL2	650	5	Fast	5.03 ± 0.01	3.0^{-17}	1	57.8	0.974
				Medium	2.53 ± 0.122	1.5^{-17}	0.5	39	
				Slow1	0.4 ± 0.8	2.3^{-18}	0.08	2.5	
				Slow2	0.03 ± 1.36	1.9^{-19}	0.006	0.3	
				Slow3	0.002 ± 0.0001	1.1^{-20}	0.0004	0.3	

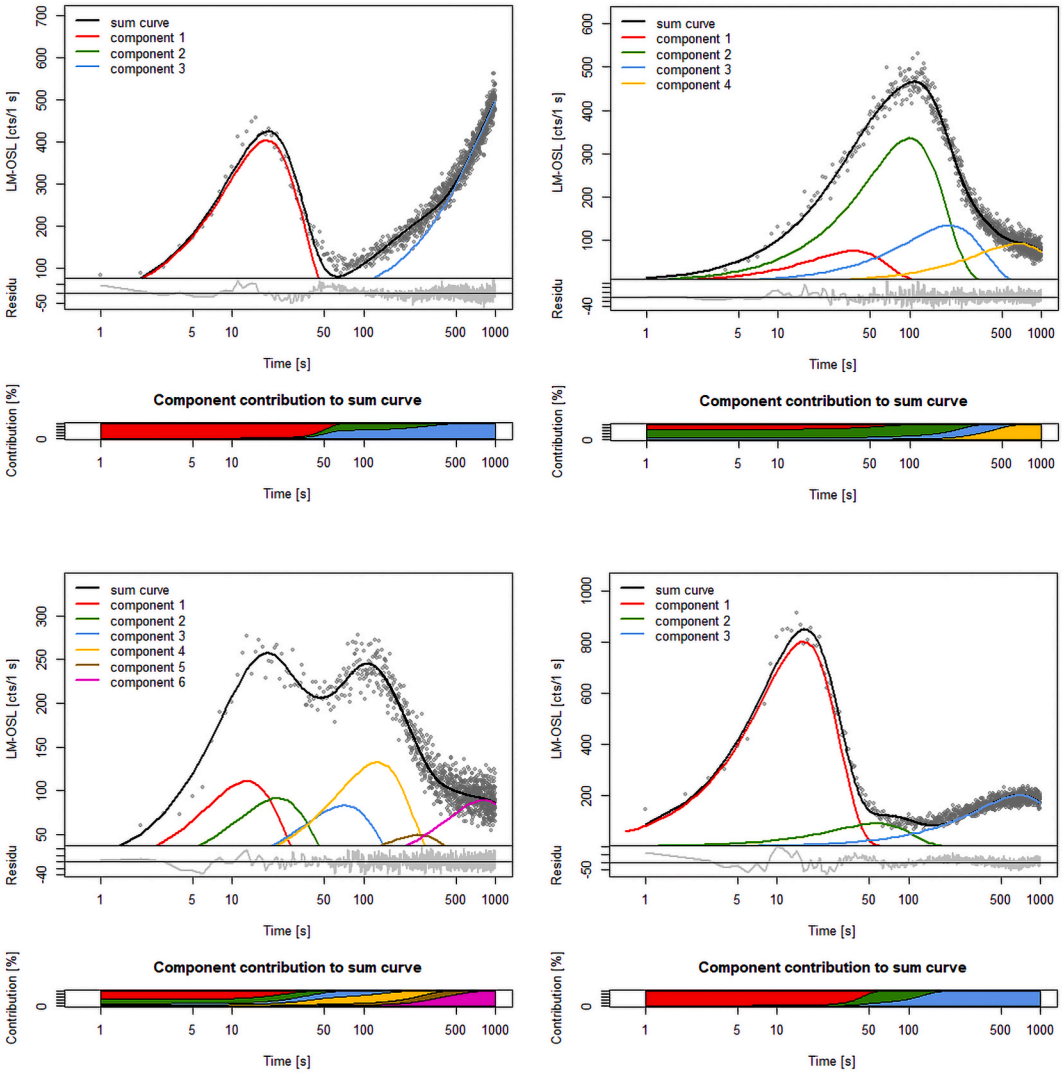

Fig. 7. LM-OSL component fitting results for Velika Vrbica samples: (A) 22172, (B) 22175, (C) 22176, and (D) 22185. Each plot shows the deconvolution of the LM-OSL signal into fast, medium, and slow components, along with their relative contributions.

spans from a depth of 11.05 m–0.05 m and is interpreted within its stratigraphic framework (Fig. 2). The results for the upper 5 m, comprising the modern soil (S0, Holocene) and the underlying loess (L1LL1), were previously presented in Perić et al. (2025a). They described a generally decreasing trend in the modern soil (S0) from ~40 $\times 10^{-8}$ m^3 kg^{-1} at its base to a minimum of ~28 $\times 10^{-8}$ m^3 kg^{-1} in the upper part of the L1LL1 loess unit at 2.95 m.

The new data reveal the complete χlf pattern for the last glacial cycle and part of the preceding interglacial. The lowermost unit, the L2 loess (below 10.60 m), shows consistently low susceptibility values, averaging around 35 $\times 10^{-8}$ m^3 kg^{-1}, which is characteristic of unweathered loess. This is overlain by the S1 palaeosol (MIS 5), recorded between approximately 8.65 m and 7.00 m, which exhibits a clear peak in χlf with values rising to 55 - 69 $\times 10^{-8}$ m^3 kg^{-1}, reflecting the enhanced pedogenesis during this interglacial period.

Above this, the L1LL2 loess (MIS 4 and lower MIS 3), extending from about 7.00 m to 5.55 m, is marked by a return to low and stable χlf values, averaging approximately 35 $\times 10^{-8}$ m^3 kg^{-1}, indicating reduced pedogenic activity. The overlying L1SS1 palaeosol (upper MIS 3) shows a moderate but distinct increase in susceptibility, with values fluctuating around 40 $\times 10^{-8}$ m^3 kg^{-1}, signifying a phase of intermediate soil formation.

The upper part of the sequence confirms the earlier findings: the L1LL1 loess (MIS 2) maintains low values, while the overlying modern soil (S0, Holocene) shows the highest susceptibility values in the profile. A prominent susceptibility peak is observed in the upper part of S0, reaching 68.7 $\times 10^{-8}$ m^3 kg^{-1} at 0.40 m, with strong fluctuations in the top meter reflecting the intensity of Holocene pedogenesis.

4.6. Comparison of quartz and K-feldspar ages

A total of 22 paired quartz OSL and K-feldspar $pIRIR_{100,290}$ ages were obtained from the loess-palaeosol sequence, spanning the Holocene soil (S0), MIS 2 loess (L1LL1), MIS 3 palaeosol (L1SS1), MIS 4 loess (L1LL2), MIS 5 palaeosol (S1) and the transition of MIS 6/MIS5 (L2). Quartz ages range from 3.0 ± 0.2 ka at the surface to 119.1 ± 8.9 ka at the base of the sequence, while corresponding K-feldspar ages vary from 5.2 ± 0.3 ka to 128.6 ± 10.3 ka (Table 1).

Across the sequence, K-feldspar ages are generally older than their quartz counterparts, with a mean K-feldspar/quartz (F/Q) ratio of 1.14 and a median of 1.06. The average offset between paired ages is +3.4 ka (median +3.7 ka). However, the degree of agreement varies systematically with stratigraphic unit. In the Holocene soil (S0), K-feldspar ages substantially exceed quartz estimates (ratios 1.4–1.7). At 10 cm depth, for instance, quartz yields 3.0 ± 0.2 ka compared to 5.2 ± 0.3 ka from K-feldspar (Fig. 8). This discrepancy is most plausibly explained by

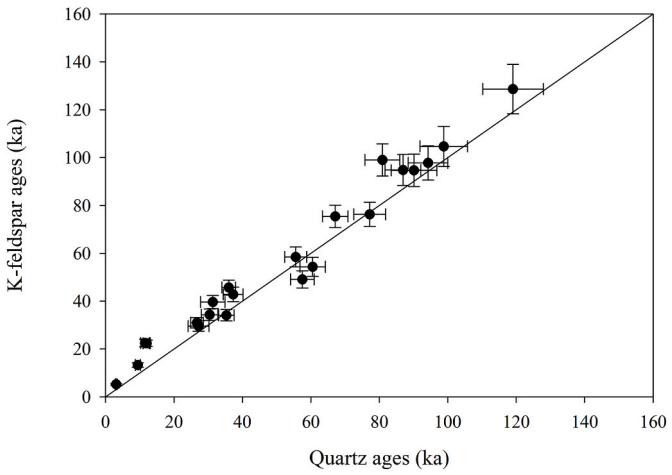

Fig. 8. Velika Vrbica LPS $pIRIR_{100,290}$ ages plotted as a function of their counterpart quartz OSL ages for the last ~127 ka. The full, diagonal line marks the ideal 1:1 ratio. The error bars denote one standard error.

incomplete bleaching of K-feldspar prior to burial. In the MIS 2 loess (L1LL1), paired ages show greater scatter. At shallower depths (100–150 cm), K-feldspar is markedly older (ratios 1.5–1.8), whereas at 200–400 cm depths, several pairs converge within error (e.g. 32.2 ± 2.6 ka quartz vs. 31.0 ± 2.2 ka K-feldspar) or even reverse, with K-feldspar slightly younger than quartz. The MIS 3 palaeosol (L1SS1) yields systematically older K-feldspar ages by 4–5 ka, but the two signals remain broadly consistent within 2σ uncertainty. In the MIS 4 loess (L1LL2), paired ages largely overlap within uncertainties, though K-feldspar tends to be 5–15 ka older at some depths (e.g. 86.9 ± 5.2 ka quartz vs. 94.8 ± 6.5 ka K-feldspar). Agreement improves toward the base of the unit. Finally, in the S1 palaeosol and the top of the L2 loess unit, quartz and K-feldspar ages are in fairly good agreement. At 1105 cm depth, for example, quartz gives 119.1 ± 8.9 ka and K-feldspar 128.6 ± 10.3 ka, consistent within errors. Overall, K-feldspar ages tend to be older than quartz ages in younger deposits (S0, L1LL1), while convergence between the two signals improves markedly in older units (L1SS1, L1LL2, S1 and L2). This pattern suggests that incomplete bleaching affects K-feldspar in young samples, whereas both minerals yield consistent burial ages in middle and late Pleistocene deposits. The difference in D_e scatter between the two signals is consistent with their bleaching characteristics. Quartz OSL D_e distributions show moderate to high overdispersion (typically 20–40 % in loess, >50 % in the youngest units), reflecting variable bleaching histories and potential micro-scale sediment mixing. By contrast, $pIRIR_{290}$ D_e values are far more homogeneous (OD mostly <15 %), underscoring the signal's more consistent resetting prior to burial. Importantly, the convergence of quartz and $pIRIR_{290}$ ages in deposits older than ~50 ka demonstrates that the higher quartz OD does not translate into systematic age offsets, affirming that both chronometers record the same burial event despite differing internal scatter.

4.7. Chronological framework for age-depth modelling

To establish a robust chronology for age-depth modelling, we evaluated the paired quartz and K-feldspar OSL ages (Table 3; Fig. 9A). As already stated, in the Holocene soil (S0) and the upper part of the MIS 2 loess (L1LL1, ≤150 cm), K-feldspar ages are consistently older than quartz by 30–80 %, most likely due to incomplete bleaching. This persistent age overestimation in younger samples suggests that the measured residual dose, despite being subtracted, may not accurately represent the true residual level in these naturally poorly bleached samples.

In the deeper part of L1LL1 (200–400 cm), quartz and K-feldspar ages generally agree within uncertainty, and weighted mean ages were calculated where possible. In the MIS 3 palaeosol (L1SS1), K-feldspar tends to yield slightly older ages (by 4–5 ka), but the offsets lie beyond the combined uncertainties; here quartz ages were retained as the preferred signal. In the MIS 4 loess (L1LL2), agreement between the two minerals improves; weighted mean ages were adopted where overlap occurs, while quartz was preferred in cases of significant divergence. In the MIS 5 palaeosol (S1), quartz and K-feldspar ages converge well within uncertainties, and weighted means of the two signals were used. Finally, for the MIS 5/MIS 6 L1 loess, the K-feldspar age was used as it showed a better agreement with the stratigraphy.

The convergence in S1 is a key finding. It demonstrates that for our quartz samples, even at ~120 ka, the signal is not in field saturation, yielding reliable and reproducible ages that are validated by an independent mineral (K-feldspar). The successful application of quartz OSL dating at Velika Vrbica up to ~120 ka contrasts with several studies

Table 3
Preferred quartz and K-feldspar ages from the Velika Vrbica loess-palaeosol sequence. Presented are also the justifications for age preferences: A - Quartz preferred; Feldspar older due to residual bleaching; B - Quartz and Feldspar agree; weighted mean used; C - Quartz preferred; Feldspar offset beyond uncertainty; D - Both signals reliable; Feldspar used - better stratigraphic consistency.

Sample id	Depth (cm)	Unit	OSL age (ka)	$pIRIR_{290}$ age (ka)	Preferred age (ka)	Justification
22172	10	S0	3.0 ± 0.2	5.2 ± 0.3	3.0 ± 0.2	A
22173	50	S0	9.3 ± 0.8	13.3 ± 0.9	9.3 ± 0.8	A
22174	100	L1LL1	15.0 ± 1.8	22.4 ± 1.3	15.0 ± 1.8	A
22175	150	L1LL1	12.4 ± 1.7	22.5 ± 1.6	12.4 ± 1.7	A
22176	200	L1LL1	32.2 ± 2.6	31.0 ± 2.2	31.6 ± 1.7	B
22177	250	L1LL1	34.2 ± 3.1	29.6 ± 2.2	31.7 ± 1.8	B
22178	300	L1LL1	32.2 ± 2.8	34.3 ± 2.4	33.2 ± 1.8	B
22179	350	L1LL1	37.4 ± 3.9	39.6 ± 2.7	38.7 ± 2.2	B
22180	400	L1LL1	35.2 ± 2.4	34.1 ± 2.4	34.7 ± 1.7	B
22181	450	L1SS1	37.9 ± 3.2	42.8 ± 3.0	37.9 ± 3.2	C
22182	500	L1SS1	41.3 ± 2.7	45.7 ± 3.1	41.3 ± 2.7	C
22183	550	L1SS1	60.5 ± 3.7	54.3 ± 4.0	60.5 ± 3.7	C
22184	600	L1LL2	57.5 ± 3.5	49.1 ± 3.6	57.5 ± 3.5	C
22185	650	L1LL2	55.6 ± 3.2	58.5 ± 4.1	56.7 ± 2.5	B
22186	700	L1LL2	67.1 ± 3.7	75.4 ± 4.7	67.1 ± 3.7	C
22187	750	L1LL2	77.2 ± 4.6	76.3 ± 5.0	76.8 ± 3.4	B
22188	800	L1LL2	86.9 ± 5.2	94.8 ± 6.5	86.9 ± 5.2	C
22189	850	L1LL2	80.9 ± 5.1	99.0 ± 6.7	80.9 ± 5.1	C
22190	900	S1	90.1 ± 6.6	94.7 ± 6.8	92.3 ± 4.7	B
22191	950	S1	94.3 ± 5.8	97.7 ± 7.2	95.8 ± 4.5	B
22192	1040	S1	98.8 ± 6.9	104.7 ± 8.4	101.5 ± 5.4	B
22193	1105	L2	119.1 ± 8.9	128.6 ± 10.3	128.6 ± 10.3	D

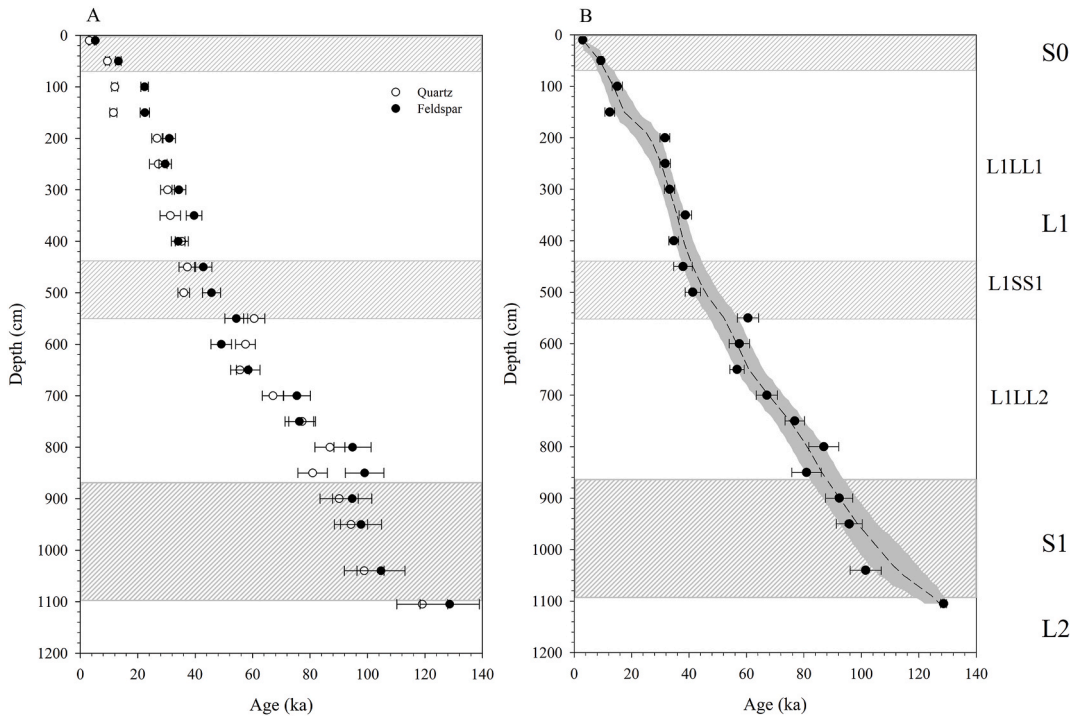

Fig. 9. A. Quartz OSL (opened circles) and K-feldspar $pIRIR_{100, 290}$ (closed circles) ages from the Velika Vrbica LPS plotted against depth. B. r. bacon age-depth model for the Velika Vrbica LPS. Black closed circles represent the luminescence ages. The grey shaded area indicates the 95 % confidence interval (minimum and maximum age limits), while the dashed line marks the mean age-depth model (see text for details).

from the wider Carpathian Basin, which report a practical upper dating limit of ~40–50 ka due to early saturation of the quartz OSL signal (e.g. Perić et al., 2019, 2022b). We attribute this to the high sensitivity and dose saturation characteristics of our quartz samples, likely resulting from a favourable provenance and sedimentary history.

This selection procedure results in a consistent age dataset in which quartz dominates the upper sequence, while deeper deposits increasingly incorporate both quartz and/or K-feldspar. The resulting "preferred ages" form the input for the age-depth modelling, ensuring that the chronology reflects stratigraphic consistency while minimizing the influence of incomplete bleaching.

The constructed rbacon age-depth model demonstrates excellent reliability and convergence (Fig. 9B). Markov Chain Monte Carlo (MCMC) mixing is very good, evidenced by a high effective sample size of 1089.5, which indicates efficient and independent sampling of the posterior distribution. There is no statistical evidence of MCMC drift (z-score = 1.92, well below the threshold of 1.96). The model's accumulation rate prior was set with a gamma shape (acc.shape) of 1.27 and a mean (acc.mean) of 112 yr/cm. The memory prior, which governs the likelihood of changes in sedimentation rate, was set with a strength (mem.strength) of 9.2 and a mean (mem.mean) of 0.49 (Fig. S2). The mean 95 % confidence ranges 9422 years, with a minimum of 1153 years at 10 cm and a maximum of 17048 years at 1030 cm depth. The resulting model depicts the temporal evolution of the sequence, with the depth-age relationship and associated uncertainties clearly defined. Crucially, 100 % of the input luminescence ages fall within the modelled age distribution, demonstrating a high degree of consistency between the dating data and the posterior model.

The resulting chronology delineates the timing of deposition and pedogenesis for each major stratigraphic unit. According to the mean rbacon model, the lowermost ~45 cm of the uncovered L2 loess unit accumulated between 127.3 and 117.1 ka. This places its deposition at the transition of MIS6/MIS5. The overlying S1 palaeosol developed between 114.7 and 88.1 ka, encompassing the late stage of MIS 5e, the stadial conditions of MIS 5d, the entire interstadial of MIS 5c, and the early part of MIS 5b, which facilitated a prolonged phase of landscape stability and pedogenesis under comparatively warmer and more humid conditions. Subsequent accumulation of the L1LL2 loess subunit occurred between 87.5 and 52.6 ka. This extensive period includes the interstadial of MIS 5a, the glacial period of MIS 4, and the early stage of MIS 3, reflecting generally cold, dry, and unstable climatic conditions throughout the Early to Mid-Pleniglacial. The intercalated L1SS1 palaeosol formed between 52.2 and 39.6 ka, within the oscillatory climate of MIS 3, representing a distinct phase of climatic amelioration and geomorphic stability. The overlying L1LL1 loess subunit was deposited between 38.9 and 11.3 ka, covering the latter part of MIS 3 and the entirety of MIS 2, including the Last Glacial Maximum. This deposition represents the main phase of Late Pleniglacial loess accumulation under peak cold and arid conditions. Finally, the modern soil (S0) has been forming since 10.8 ka, corresponding to the Holocene (MIS 1).

4.8. Dust mass accumulation rates

Calculated dust mass accumulation rates (MARs) for the Velika Vrbica LPS, using the same calculation method as described by Perić et al. (2025a, 2025b), are shown in Fig. 10 and Table S4. The MAR values exhibit significant fluctuations throughout the investigated time period, reflecting changing dust influx dynamics. The results for the upper 500 cm (approximately the last 45 ka) were previously presented in Perić et al. (2025a), noting high MARs during MIS 3 and variable but generally lower rates during MIS 2 and the Holocene (MIS 1). The new data from the lower part of the sequence reveal the dust accumulation history back to approximately 127 ka. The lowermost unit, the L2 loess (MIS 4), shows moderate MAR values, averaging around 70 g m^{-2} a^{-1}. A significant shift occurs with the onset of the S1 palaeosol (MIS 5), where MAR values decrease markedly to an average of 110 g m^{-2} a^{-1}, indicating reduced dust deposition during this interglacial period. This low dust flux persists into the overlying L1LL2 loess (early MIS 4 and MIS 3), which records the lowest sustained MARs in the profile, averaging 125 g

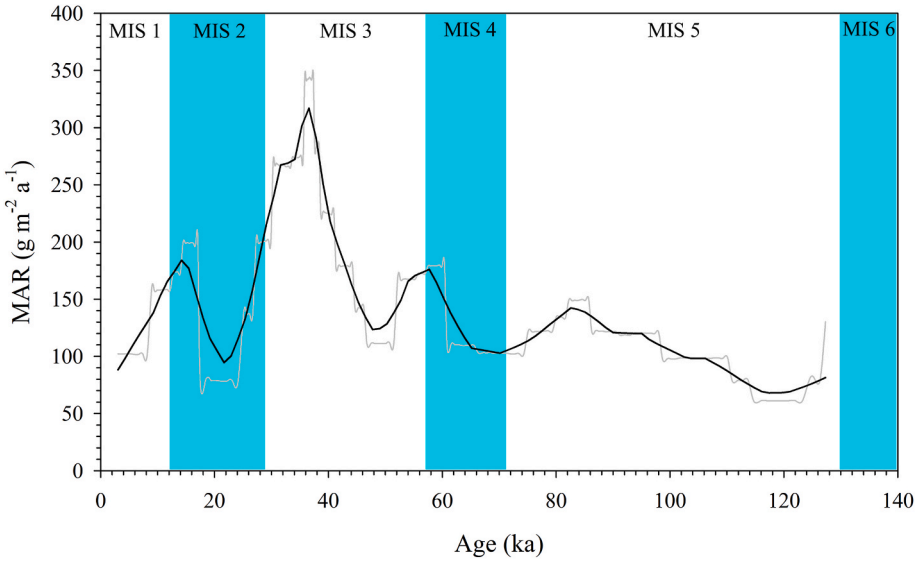

Fig. 10. Dust mass accumulation rates (MARs) for the Velika Vrbica, LPSs shown as functions of age. The MARs are based on mean ages with 95 % confidence intervals. For a more realistic representation the values were smoothed using the LOESS method (tricube weighting, polynomial regression, SigmaPlot 11.0; sampling proportion = 0.100, polynomial degree = 1). The full black line represents the smoothed values, while the full grey line shows the raw, unsmoothed MARs.

m^{-2} a^{-1}. The overlying L1SS1 palaeosol (mid to late MIS 3) shows a pronounced increase in dust accumulation, with MARs rising to an average of 185 g m^{-2} a^{-1}, confirming the peak dust deposition previously identified for this period. This is followed by the L1LL1 loess (MIS 2), which displays a variable but generally high mean MAR of 168 g m^{-2} a^{-1}, characterized by significant fluctuations between maximum values near 190 g m^{-2} a^{-1} and minima around 145 g m^{-2} a^{-1}. The modern soil (S0, Holocene, MIS 1) displays the lowest mean MAR values, averaging 138 g m^{-2} a^{-1}, consistent with the termination of full glacial conditions. Overall, the record demonstrates that the highest dust accumulation occurred during the periods of MIS 2 and MIS 3, while the lowest rates are associated with the interglacial soils (S1 and S0).

5. Discussion

The integrated luminescence chronology and multi-proxy dataset from the Velika Vrbica LPS provide a robust framework for reconstructing environmental dynamics in the Wallachian Basin from MIS 5 to the Holocene. The following discussion evaluates the performance of the luminescence signals with a particular focus on the LM-OSL results, interprets the stratigraphic and chronological record, and places the findings within the broader context of regional palaeoclimate.

5.1. Performance and reliability of luminescence signals

A primary objective of this study was to evaluate the applicability of quartz OSL and K-feldspar $pIRIR_{290}$ signals for dating a long, continuous loess-palaeosol sequence. Our results demonstrate a clear and systematic pattern in the agreement between the two chronometers. In the younger deposits (S0 and upper L1LL1, ≤150 cm), K-feldspar ages are consistently older than their quartz counterparts by 30–80 % (F/Q ratio: 1.4–1.8). This discrepancy can, most likely, be attributed to incomplete bleaching of the K-feldspar signal prior to burial, a well-documented issue in aeolian and fluvial settings (e.g., Buylaert et al., 2011). The $pIRIR_{290}$ signal is known to be more difficult to bleach completely than the quartz OSL signal, and our residual dose correction, while methodologically robust, may represent a minimum estimate for samples deposited under sub-optimal bleaching conditions. Consequently, for the Holocene and upper Last Glacial loess, the quartz OSL ages are considered more reliable. Conversely, for deposits older than ~50 ka, particularly within the L1LL2 loess and the S1 palaeosol, the quartz and K-feldspar ages converge to within uncertainties. This excellent agreement has two critical implications. First, it confirms the reliability of quartz OSL ages beyond the commonly cited regional saturation limit of ~40–60 ka (e.g. Avram et al., 2020; Perić et al., 2019, 2022b; Stevens et al., 2011) and even beyond the limits reported for Chinese loess, where Buylaert et al. (2007) suggested that quartz dating should generally be restricted to samples younger than ~70 ka (preferably younger than 40–50 ka) corresponding to a D_e of ~200 Gy. The high sensitivity and favourable dose saturation characteristics of the quartz from Velika Vrbica suggest a provenance and sedimentary history that has preserved a luminescence signal capable of accurately recording burial doses up to ~300 Gy. Second, the convergence indicates that the $pIRIR_{290}$ signal from K-feldspar in these older units is stable and unaffected by significant anomalous fading. The close correspondence between the two independent mineral signals provides strong empirical evidence for the robustness of the chronology for the end of the middle and late Pleistocene parts of the sequence, eliminating the need for model-dependent fading corrections that rely on untestable assumptions (Buylaert et al., 2012).

5.2. Insights from LM-OSL component analysis

The LM-OSL results provide a deeper, grain-specific insight into the luminescence properties of the quartz fraction. The overwhelming dominance of the fast component (>85–90 %) throughout the majority of the profile is a key finding. It confirms that the quartz grains are generally well-bleached and possess a favourable trap structure, making them highly suitable for equivalent dose determination using standard SAR protocols. The high pseudo-R^2 values (0.92–0.98) affirm the robustness of the deconvolution and the reliability of the component analysis (Table S1). The anomalous component distributions observed at specific depths (150 cm, 200 cm, and 650 cm) are particularly useful. We theorize that these deviations are not analytical artefacts but reflect genuine changes in sedimentological history or provenance. The significant reduction in the fast component (56 %) and the increased contribution of medium (27 %) and slow components at 200 cm (sandy layer within L1LL1), likely indicate a different sediment source for this sandy intercalation. Coarser, sandy layers often originate from more proximal sources or different transport pathways (e.g., river channel or sand sheet deposits) compared to the typical silty loess. This shift in provenance could introduce quartz grains with a different geological

history and, consequently, a different trap population structure, characterized by a higher proportion of less stable (medium and slow) components. The anomalously high b-value (6.05) at this depth further supports a distinct mineralogical or physical characteristic of the quartz grains in this layer. The dominance of the medium component (55 % and 39 %, respectively) at 150 cm (L1LL1) and 650 cm (L1LL2) is more ambiguous. One plausible explanation is sediment reworking or incomplete bleaching prior to final deposition. During reworking, grains may be exposed to limited light, sufficient to bleach the most light-sensitive (fast) electrons but not the more persistent charges in medium and slow traps. This would result in a relative enrichment of the medium component in the natural signal, as observed. Alternatively, these horizons may represent periods of significantly reduced sedimentation rates or pedogenic alteration that subtly altered the crystal lattice of the quartz grains, perhaps through dissolution and reprecipitation, thereby affecting the relative stability of different traps. The very low fast component b-value at 150 cm (0.72) suggests a fundamental difference in the detrapping probability, consistent with either a change in the physical characteristics of the grains or a complex bleaching history.

The stability of the fast component in the palaeosols (L1SS1 and S1) is noteworthy. Despite intense pedogenesis, which can alter mineral surfaces, the quartz OSL signals remain dominated by the fast component. This suggests that the pedogenic processes affecting this sequence did not fundamentally reset or alter the luminescence trap properties of the quartz grains to an extent that would compromise dating reliability.

5.3. Chronostratigraphy and regional correlation

The Bayesian age-depth model provides a continuous and internally consistent chronology that allows for a detailed interpretation of the depositional and pedogenic history. The model successfully integrates the preferred luminescence ages, respecting stratigraphic superposition and resulting in a reliable accumulation history with well-constrained uncertainty envelopes. The deposition of the uppermost ~45 cm of the L2 loess is dated at the transition of MIS6/MIS5. This aligns with findings from other sites in the Carpathian Basin. At Crvenka, Stevens et al. (2011) reported 114 ± 7 ka for the upper L2 loess. At Stari Slankamen, Schmidt et al. (2010) obtained 193–100 ka for the L2 at, while Murray et al. (2014) reported 170 ± 13 ka from a sample above an erosion surface. Most recently, Perić et al. (2022) dated the L2 loess at Irig between 121 and 174 ka. The development of the S1 palaeosol between ~115 and 88 ka aligns well with the MIS 5 interglacial complex. This prolonged period of pedogenesis, encompassing MIS 5e through to early MIS 5b, indicates extended landscape stability under generally warmer and more humid conditions than the subsequent glacial stages. The timing is consistent with S1 palaeosols recorded in other loess sequences across the Danube Basin and the Carpathian region (Marković et al., 2015; Constantin et al., 2019), supporting the regional synchronicity of this prominent pedostratigraphic marker. This interpretation is further supported by luminescence-dated LPS in the Vojvodina region, including Orlovat (Marković et al., 2014), Crvenka (Stevens et al., 2011), and Stari Slankamen (Murray et al., 2014), Irig (Perić et al., 2022a) where the S1 has been dated to ~120–60 ka.

The overlying L1LL2 loess subunit, deposited between ~88 and 53 ka, records the transition into and persistence of glacial conditions during MIS 4 and early MIS 3. The overprinting of this unit by pedogenic processes, as suggested by the elevated radionuclide concentrations, indicates that it is not a primary loess deposit but has likely been significantly reworked or altered. This complicates a straightforward interpretation but highlights the dynamic nature of sedimentation during the Early to Mid-Pleniglacial.

The formation of the L1SS1 palaeosol between ~52 and 40 ka during MIS 3 represents a distinct phase of climatic amelioration within the last glacial cycle. This interstadial soil is a key stratigraphic marker across South-eastern Europe, and its identification at Velika Vrbica reinforces its regional importance. Similar ages for upper palaeosols have been reported from several LPS in the Vojvodina region, including Surduk (31.8 ± 3.7 ka; (Fuchs et al., 2008), Stari Slankamen (34.4 ± 2.2 ka; Schmidt et al., 2010), Crvenka (38 ± 4 ka; Stevens et al., 2011), Veliki Surduk on the Titel loess plateau (34.2 ± 2.4 ka; Perić et al., 2019), and Irig (23–63 ka; Perić et al., 2022a). Taken together, these results broadly agree with the ~52–40 ka range established at Velika Vrbica, although some variability exists, most likely due to methodological differences, local sedimentation dynamics, and potential erosional or reworking processes affecting the preservation of palaeosols. Importantly, the correspondence extends beyond the Vojvodina region, as shown by the uppermost intercalated soil at the Nosak LPS in northeastern Serbia, which yielded an age of 31 ± 4 ka (Perić et al., 2020), albeit representing a less well-developed pedogenic horizon. The overall agreement across sites underscores the regional significance of L1SS1 as a stratigraphic marker of MIS 3 interstadial conditions, even though site-specific factors may account for minor discrepancies in the exact timing. The overlying L1LL1 loess, deposited from ~39 ka through the Last Glacial Maximum (MIS 2), represents the main phase of Late Pleniglacial loess accumulation under peak cold and arid conditions. The uppermost loess layer, L1LL1, has been dated at several sites in the Carpathian Basin and consistently points to deposition during MIS 2. At Irig, Perić et al. (2022) reported ages between 10.2 ± 0.7 and 24.4 ± 1.7 ka, while at Stari Slankamen comparable ages of 23.3 ± 1.5 and 23.6 ± 1.4 ka were obtained (Schmidt et al., 2010; Murray et al., 2014). At Veliki Surduk, high-resolution quartz dating further constrained L1L1 deposition to between 15.6 ± 1.2 and 29.8 ± 5.8 ka (Perić et al., 2019), at the Novo Orahovo LP, the same layer was dated at 23.8 ± 0.7 ka (Marković et al., 2023) while at the Požarevac site (north-eastern Serbia) the age was determined to be 22.2 ± 2.2 ka (Marković et al., 2021; Perić et al., 2021). Taken together, these results demonstrate good agreement in placing the L1LL1 loess within MIS 2, although minor discrepancies in the onset and duration of deposition are evident between sites. These differences likely reflect variations in sedimentation rates, local geomorphological conditions, or sampling resolution. Nonetheless, the combined chronology confirms that the L1LL1 unit represents the terminal phase of loess accumulation prior to the onset of Holocene soil formation. Finally, the S0 Holocene soil at the Velika Vrbica LPS has been developing since 10.8 ka, marking the onset of pedogenesis under interglacial conditions. Comparable ages have been obtained from other sites in the neighbouring Carpathian Basin: 7.1 ± 0.5 ka at Irig (Perić et al., 2022a), 7.7 ± 0.6 ka at Crvenka (Stevens et al., 2011), 7.4 ± 0.7 ka at Veliki Surduk (Perić et al., 2019), 7.3 ± 0.4 ka at Stari Slankamen (Murray et al., 2014) and 6.7 ± 0.5 ka at Kisiljevo (Perić et al., 2022a, 2024). While the Velika Vrbica age is slightly older than those reported at neighbouring sites, the overall agreement supports a broadly synchronous onset of Holocene soil formation across the region. The reason for the minor offsets is most likely the same as for the underlying units (local differences in pedogenic intensity, sediment reworking, dating resolution etc.) but collectively the data confirm the S0 soil as a consistent marker of Holocene environmental stability throughout the Middle and Lower Danube Basin.

The chronology demonstrates that the Velika Vrbica sequence provides a nearly continuous record that captures the major glacial-interglacial and stadial-interstadial cycles of the last ~130 ka, making it a key archive for the lower Danube basin.

5.4. Palaeoenvironmental implications and dust accumulation

The magnetic susceptibility (χlf) record serves as a proxy for pedogenic intensity and generally correlates well with the established stratigraphy. The low χlf values in the loess units (L2, L1LL2, and the lower part of L1LL1) reflect weak pedogenesis under dry glacial conditions, while the pronounced peaks in the S1 and S0 palaeosols signal enhanced magnetic mineral formation during interglacial periods. The moderate increase in χlf within the L1SS1 palaeosol is characteristic of the less

intense weathering typical of interstadial soils.

The MARs derived from the age-depth model indicate fluctuating dust influx dynamics. In this study, MARs derived from the age-depth model reveal a distinct pattern, with the highest values observed during MIS 3. This finding is notable as it does not agree with the accepted dust deposition model, which typically associates peak accumulation with the most severe glacial conditions of MIS 2 (e.g. Kohfeld and Harrison, 2003, 2001; Stevens et al., 2011; Zhang et al., 1999). Similar high MARs during MIS 3 were reported for a number of sites in the neighbouring Carpathian Basin, most notably for the LPS Nosak, Kisiljevo, Belotinac, and Surduk (e.g. Basarin et al., 2011; Fuchs et al., 2008; Perić et al., 2025a, 2025b, 2024, 2022, 2020). The lowest MARs correspond to the pedogenically stable intervals of MIS 5 and the Holocene (S1 and S0 soils), reflecting reduced dust availability and increased vegetation stabilization, which aligns with the general model of loess-palaeosol formation where dust accumulation and soil development are anti-correlated (e.g. Frechen et al., 2003; Kohfeld and Harrison, 2003, 2001). The pronounced high MARs during MIS 3, consistent with Carpathian Basin records (Perić et al., 2025a, 2025b), suggest that dust deposition in the Wallachian Basin was not solely driven by global ice volume but was also intensified during certain interstadial phases. This points to the influence of regional atmospheric circulation patterns and sediment supply dynamics that can decouple dust influx from the global glacial maximum.

6. Conclusions

This study establishes Velika Vrbica as one of the most thoroughly dated loess-palaeosol sequences in the lower Danube basin, providing a high-resolution chronological framework that spans from MIS 5 to the present. The evaluation of quartz OSL and K-feldspar $pIRIR_{290}$ signals demonstrates that, with careful assessment of bleaching histories, both minerals can yield reliable ages beyond 100 ka in this setting. The convergence of the two signals in older deposits is a significant finding, challenging the notion that quartz OSL is inherently limited to the last ~50 ka in the region. The LM-OSL analysis provides critical support for the reliability of the quartz signals and offers insights into sediment dynamics. The dominant fast component confirms the general suitability of the quartz for dating, while the anomalous horizons likely mark periods of sedimentological change, such as shifts in provenance (e.g., the sandy layer at 200 cm) or episodes of reworking and partial bleaching (e.g., at 150 cm and 650 cm). These results highlight the value of LM-OSL as a tool for assessing the internal consistency of a luminescence chronology and for identifying stratigraphic complexities that may not be apparent from D_e values alone. The resulting chronology reveals a detailed history of loess accumulation and soil formation that correlates well with global marine isotope stages and regional climate records. The sequence reliably records the major climatic shifts of the last glacial-interglacial cycle, providing a valuable terrestrial archive for Southeastern Europe. These findings contribute to the refinement of the temporal framework for the Wallachian Basin and contribute to the broader methodological discussions on the limits and application of luminescence dating in long Quaternary sediment records. The demonstrated robustness of the signals at Velika Vrbica underscores the importance of site-specific testing and supports the use of multi-mineral, multi-protocol approaches for constructing reliable chronologies in complex loess-palaeosol sequences.

CRediT authorship contribution statement

Zoran M. Perić: Writing – review & editing, Writing – original draft, Visualization, Validation, Supervision, Software, Resources, Project administration, Methodology, Investigation, Funding acquisition, Formal analysis, Data curation, Conceptualization. **Cathal S. Ryan:** Writing – review & editing, Resources, Methodology, Investigation, Formal analysis, Data curation. **Milica G. Bosnić:** Writing – review & editing, Validation, Resources, Methodology, Investigation, Data curation. **Petar Krsmanović:** Writing – review & editing, Visualization, Resources, Investigation, Data curation. **Warren Thompson:** Writing – review & editing, Validation, Methodology, Investigation, Formal analysis, Data curation. **Helena Alexanderson:** Writing – review & editing, Validation, Methodology, Investigation, Formal analysis. **Slobodan B. Marković:** Writing – review & editing, Validation, Supervision, Resources, Methodology, Investigation, Conceptualization.

Declaration of competing interest

The authors declare that they have no known competing financial interests or personal relationships that could have appeared to influence the work reported in this paper.

Acknowledgments

The research of ZMP on Danube Basin loess chronology was funded by the Royal Physiographic Society in Lund (grants 42788 and 43046). SBM acknowledges the Silesian Technical University Professorship, awarded under the Excellence Initiative - Research University Programme. MGB received support from the L' Oréal-UNESCO For Women in Science award and Western Balkan 6 –Visegrad 4 Fellowship #62470105. Furthermore, this work is part of the project "The Loess Plateau Margins: Towards Innovative Sustainable Conservation - LAMINATION" (#17807), funded by the Science Fund of the Republic of Serbia. All experimental work was carried out at the Lu^2D^2 infrastructure (The Lund Luminescence centre for Dating and Dosimetry). SBM and MGB gratefully acknowledge the financial support of the Ministry of Science, Technological Development and Innovation of the Republic of Serbia (Grants No. 451-03-137/2025–03/200125 & 451-03-136/2025–03/200125).

Appendix A. Supplementary data

Supplementary data to this article can be found online at https://doi.org/10.1016/j.quageo.2026.101726.

Data availability

Data will be made available on request.

References

Adamiec, G., Aitken, M.J., 1998. Dose-rate conversion factors: update. Ancient tL 16, 37–50.
Adamiec, G., 2005. OSL decay curves—relationship between single-and multiple-grain aliquots. Radiat. Meas. 39, 63–75.
Avram, A., Constantin, D., Veres, D., Kelemen, S., Obreht, I., Hambach, U., Marković, S. B., Timar-Gabor, A., 2020. Testing polymineral post-IR IRSL and quartz SAR-OSL protocols on Middle to late Pleistocene loess at Batajnica, Serbia. Boreas 49, 615–633. https://doi.org/10.1111/bor.12442.
Bailey, S.D., Wintle, A.G., Duller, G.A.T., Bristow, C.S., 2001. Sand deposition during the last millennium at Aber!raw, Anglesey, North Wales as determined by OSL dating of quartz. Quat. Sci. Rev. 4.
Balian, H.G., Eddy, N.W., 1977. Figure-of-merit (FOM), an improved criterion over the normalized chi-squared test for assessing goodness-of-fit of gamma-ray spectral peaks. Nucl. Instrum. Methods 145, 389–395.
Basarin, B., Vandenberghe, D.A.G., Marković, S.B., Catto, N., Hambach, U., Vasiliniuc, S., Derese, C., Ronĉević, S., Vasiljević, D.A., Rajić, L., 2011. The Belotinac section (Southern Serbia) at the southern limit of the European loess belt: initial results. Quat. Int. 240, 128–138. https://doi.org/10.1016/J.QUAINT.2011.02.022.
Bell, W.T., 1980. Alpha dose attenuation in quartz grains for thermoluminescence dating. Ancient Tl 12, 4–8.
Blaauw, M., Christen, J.A., 2011. Flexible paleoclimate age-depth models using an autoregressive gamma process. Bayesian Analysis 6, 457–474. https://doi.org/10.1214/11-BA618.
Bøtter-Jensen, L., Andersen, C.E., Duller, G.A.T., Murray, A.S., 2003. Developments in radiation, stimulation and observation facilities in luminescence measurements. Radiat. Meas. 37, 535–541. https://doi.org/10.1016/S1350-4487(03)00020-9.
Brennan, B.J., Lyons, R.G., Phillips, S.W., 1991. Attenuation of alpha particle track dose for spherical grains. International Journal of radiation applications and

instrumentation. Part D. Nucl. Tracks Radiat. Meas. 18, 249–253. https://doi.org/10.1016/1359-0189(91)90119-3.
Buggle, B., Glaser, B., Zöller, L., Hambach, U., Marković, S., Glaser, I., Gerasimenko, N., 2008. Geochemical characterization and origin of Southeastern and Eastern European loesses (Serbia, Romania, Ukraine). Quat. Sci. Rev. 27, 1058–1075. https://doi.org/10.1016/J.QUASCIREV.2008.01.018.
Buggle, B., Hambach, U., Kehl, M., Marković, S.B., Zöller, L., Glaser, B., 2013. The progressive evolution of a continental climate in southeast-central European lowlands during the Middle Pleistocene recorded in loess paleosol sequences. Geology 41, 771–774. https://doi.org/10.1130/G34198.1.
Bulur, E., 1996. An alternative technique for optically stimulated luminescence (OSL) experiment. Radiat. Meas. 26, 701–709. https://doi.org/10.1016/S1350-4487(97)82884-3.
Buylaert, J.-P., Jain, M., Murray, A.S., Thomsen, K.J., Thiel, C., Sohbati, R., 2012. A robust feldspar luminescence dating method for middle and Late Pleistocene sediments. Boreas 41, 435–451. https://doi.org/10.1111/j.1502-3885.2012.00248.x.
Buylaert, J.-P., Thiel, C., Murray, A.S., Vandenberghe, D.A., Yi, S., Lu, H., 2011. IRSL and post-IR IRSL residual doses recorded in modern dust samples from the Chinese Loess Plateau. Geochronometria 38, 432–440.
Buylaert, J.P., Vandenberghe, D., Murray, A.S., Huot, S., De Corte, F., Van den Haute, P., 2007. Luminescence dating of old (>70 ka) Chinese loess: a comparison of single-aliquot OSL and IRSL techniques. Quat. Geochronol. 2, 9–14. https://doi.org/10.1016/J.QUAGEO.2006.05.028.
Constantin, D., Veres, D., Panaiotu, C., Anechitei-Deacu, V., Groza, S.M., Begy, R., Kelemen, S., Buylaert, J.P., Hambach, U., Marković, S.B., Gerasimenko, N., Timar-Gabor, A., 2019. Luminescence age constraints on the Pleistocene-Holocene transition recorded in loess sequences across SE Europe. Quaternary Geochronology 49, 71–77. https://doi.org/10.1016/J.QUAGEO.2018.07.011.
Duller, G.A.T., 2015. The Analyst software package for luminescence data: overview and recent improvements. Ancient TL 33, 35–42.
Durcan, J.A., King, G.E., Duller, G.A.T., 2015. DRAC: Dose Rate and Age Calculator for trapped charge dating. Quat. Geochronol. 28, 54–61. https://doi.org/10.1016/j.quageo.2015.03.012.
Frechen, M., Oches, E.A., Kohfeld, K.E., 2003. Loess in Europe - mass accumulation rates during the last glacial period. Quat. Sci. Rev. 22, 1835–1857. https://doi.org/10.1016/S0277-3791(03)00183-5.
Fuchs, M., Rousseau, D.D., Antoine, P., Hatté, C., Gauthier, C., Marković, S., Zoeller, L., 2008. Chronology of the last climatic cycle (Upper Pleistocene) of the Surduk loess sequence, Vojvodina, Serbia. Boreas 37, 66–73. https://doi.org/10.1111/J.1502-3885.2007.00012.X.
Gallet, S., Jahn, B.M., Torii, M., 1996. Geochemical characterization of the Luochuan loess-paleosol sequence, China, and paleoclimatic implications. Chem. Geol. 133, 67–88. https://doi.org/10.1016/S0009-2541(96)00070-8.
Guérin, G., Mercier, N., Adamiec, G., 2011. Dose-rate conversion factors: update. Ancient Tl 29, 5–8.
Guérin, G., Mercier, N., Nathan, R., Adamiec, G., Lefrais, Y., 2012. On the use of the infinite matrix assumption and associated concepts: a critical review. Radiation measurements. Proceedings of the 13th International Conference on Luminescence and Electron Spin Resonance Dating, 10–14 July, 2011, Toruń, Poland 47, 778–785. https://doi.org/10.1016/j.radmeas.2012.04.004.
Hansen, V., Murray, A., Buylaert, J.-P., Yeo, E.-Y., Thomsen, K., 2015. A new irradiated quartz for beta source calibration. Radiat. Meas. 81, 123–127. https://doi.org/10.1016/j.radmeas.2015.02.017.
Huntley, D.J., Baril, M., 1997. The K content of the K-feldspars being measured in optical dating or in thermoluminescence dating. Ancient Tl 15, 11–13.
Huntley, D.J., Hancock, R., Ancient, T., 2001. The Rb contents of the K-feldspar grains being measured in optical dating. ancient TL 19, 43–46.
Jordanova, D., Simon, Q., Balescu, S., Jordanova, N., Ishlyamski, D., Georgieva, B., Bourlès, D.L., Duvivier, A., Cornu, S., 2022. Environmental changes in southeastern Europe over the last 450 ka: magnetic and pedologic study of a loess-paleosol profile from Kaolinovo (Bulgaria). Quat. Sci. Rev. 292, 107671. https://doi.org/10.1016/j.quascirev.2022.107671.
Kars, R.H., Reimann, T., Ankjærgaard, C., Wallinga, J., 2014. Bleaching of the post-IR IRSL signal: new insights for feldspar luminescence dating. Boreas 43, 780–791. https://doi.org/10.1111/bor.12082.
Kemp, R.A., 2001. Pedogenic modification of loess: significance for palaeoclimatic reconstructions. Earth-Science Reviews, Recent research on loess and palaeosols, pure and applied 54, 145–156. https://doi.org/10.1016/S0012-8252(01)00045-9.
Kitis, G., Pagonis, V., 2008. Computerized curve deconvolution analysis for LM-OSL. Radiat. Meas. 43, 737–741. https://doi.org/10.1016/j.radmeas.2007.12.055.
Kitis, G., Polymeris, G.S., Kiyak, N.G., Pagonis, V., 2011. Preliminary results towards the equivalence of transformed continuous-wave optically stimulated luminescence (CW-OSL) and linearly-modulated (LM-OSL) signals in quartz. Geochronometria 38, 209–216.
Kohfeld, K.E., Harrison, S.P., 2003. Glacial-interglacial changes in dust deposition on the Chinese Loess Plateau. Quat. Sci. Rev. 22, 1859–1878. https://doi.org/10.1016/S0277-3791(03)00166-5.
Kohfeld, K.E., Harrison, S.P., 2001. DIRTMAP: the geological record of dust. Earth Sci. Rev. 54, 81–114. https://doi.org/10.1016/S0012-8252(01)00042-3.
Kolb, T., Tudyka, K., Kadereit, A., Lomax, J., Poręba, G., Zander, A., Zipf, L., Fuchs, M., 2022. The μDose system: determination of environmental dose rates by combined alpha and beta counting – performance tests and practical experiences. Geochronology 4, 1–31. https://doi.org/10.5194/gchron-4-1-2022.
Kreutzer, S., Schmidt, C., Fuchs, M.C., Dietze, M., Fischer, M., Fuchs, M., 2012. Introducing an R package for luminescence dating analysis. Ancient TL 30, 1–8.
Krsmanović, P., Perić, Z.M., Thompson, W., Radaković, M.G., Ryan, C.S., Schaetzl, R.J., Hao, Q., Lukić, T., Alexanderson, H., Marković, S.B., 2025. Loess provenance in the westernmost part of the lower danube basin, Serbia: geochemical insights from the Velika Vrbica fluvial–eolian section. Quat. Int. 748, 109969. https://doi.org/10.1016/j.quaint.2025.109969.
Li, B., Li, S.-H., 2011. Luminescence dating of K-feldspar from sediments: a protocol without anomalous fading correction. Quat. Geochronol. 6, 468–479.
Liu, T., 1985. Loess and the Environment: Beijing. China Ocean Press, pp. 18–28.
Marković, S.B., Oches, E.A., Perić, Z.M., Gaudenyi, T., Jovanović, M., Sipos, G., Thiel, C., Buylaert, J.-P., Savić, S., Mccoy, W.D., Radaković, M.G., Marković, R.S., Gavrilov, M. B., 2021. The Požarevac loess-paleosol sequence: a record of increased aridity in the south-eastern margin of the Carpathian basin during the last 350 ka. J. Quat. Sci. 1436–1447. https://doi.org/10.1002/jqs.3327.
Marković, S.B., Stevens, T., Kukla, G.J., Hambach, U., Fitzsimmons, K.E., Gibbard, P., Buggle, B., Zech, M., Guo, Z., Hao, Q., Wu, H., O'Hara Dhand, K., Smalley, I.J., Újvári, G., Sümegi, P., Timar-Gabor, A., Veres, D., Sirocko, F., Vasiljević, D.A., Jary, Z., Svensson, A., Jović, V., Lehmkuhl, F., Kovács, J., Svirčev, Z., 2015. Danube loess stratigraphy — towards a Pan-European loess stratigraphic model. Earth Sci. Rev. 148, 228–258. https://doi.org/10.1016/J.EARSCIREV.2015.06.005.
Marković, S.B., Timar-Gabor, A., Stevens, T., Hambach, U., Popov, D., Tomić, N., Obreht, I., Jovanović, M., Lehmkuhl, F., Kels, H., Marković, R., Gavrilov, M.B., 2014. Environmental dynamics and luminescence chronology from the Orlovat loess-palaeosol sequence (Vojvodina, northern Serbia). J. Quat. Sci. 29, 189–199. https://doi.org/10.1002/JQS.2693.
Marković, S.B., Vandenberghe, J., Perić, Z.M., Filyó, D., Bartyik, T., Radaković, M.G., Hao, Q., Marković, R.S., Lukić, T., Tomić, N., Gavrilov, M.B., Antić, A., Cvijanović, I., Sipos, G., 2023. Local differentiation in the loess deposition as a function of dust source: key study novo Orahovo loess Paleosol sequence (Vojvodina, Serbia). Quaternary 6, 23. https://doi.org/10.3390/quat6010023.
Mejdahl, V., 1987. Internal radioactivity in quartz and feldspar grains. Ancient TL 5, 10–17.
Murray, A., Marten, R., Johnston, A., Martin, P., 2005. Analysis for naturally occurring radionuclides at environmental concentrations by gamma spectrometry. https://doi.org/10.1007/bf02037443.
Murray, A.S., Schmidt, E.D., Stevens, T., Buylaert, J.P., Marković, S.B., Tsukamoto, S., Frechen, M., 2014. Dating Middle Pleistocene loess from Stari Slankamen (Vojvodina, Serbia) — limitations imposed by the saturation behaviour of an elevatd temperature IRSL signal. Catena 117, 34–42. https://doi.org/10.1016/J.CATENA.2013.06.029.
Murray, A.S., Wintle, A.G., 2003. The single aliquot regenerative dose protocol: potential for improvements in reliability. Radiat. Meas. 37, 377–381. https://doi.org/10.1016/S1350-4487(03)00053-2.
Murray, A.S., Wintle, A.G., 2000. Luminescence dating of quartz using an improved single-aliquot regenerative-dose protocol. Radiat. Meas. 32, 57–73. https://doi.org/10.1016/S1350-4487(99)00253-X.
Peng, J., Dong, Z., Han, F., Han, Y., Dai, X., 2014. Estimating the number of components in an OSL decay curve using the Bayesian information Criterion. Geochronometria 41, 334–341.
Perić, Z., Lagerbäck Adolphi, E., Stevens, T., Újvári, G., Zeeden, C., Buylaert, J.P., Marković, S.B., Hambach, U., Fischer, P., Schmidt, C., Schulte, P., Huayu, L., Shuangwen, Y., Lehmkuhl, F., Obreht, I., Veres, D., Thiel, C., Frechen, M., Jain, M., Vött, A., Zöller, L., Gavrilov, M.B., 2019. Quartz OSL dating of late quaternary Chinese and Serbian loess: a cross Eurasian comparison of dust mass accumulation rates. Quat. Int. 502, 30–44. https://doi.org/10.1016/J.QUAINT.2018.01.010.
Perić, Z.M., Marković, S.B., Avram, A., Timar-Gabor, A., Zeeden, C., Nett, J.J., Fischer, P., Fitzsimmons, K.E., Gavrilov, M.B., 2022a. Initial quartz OSL and dust mass accumulation rate investigation of the Kisiljevo loess sequence in north-eastern Serbia. Quat. Int. 620, 13–23. https://doi.org/10.1016/J.QUAINT.2020.10.040.
Perić, Z.M., Marković, S.B., Filyó, D., Thiel, C., Murray, A.S., Gavrilov, M.B., Nett, J.J., Sipos, G., 2021. Quartz OSL and polymineral post IR–IRSL dating of the Požarevac loess–palaeosol sequence in north–eastern Serbia. Quat. Geochronol. 66, 101216. https://doi.org/10.1016/J.QUAGEO.2021.101216.
Perić, Z.M., Marković, S.B., Sipos, G., Gavrilov, M.B., Thiel, C., Zeeden, C., Murray, A.S., 2020. A post-IR IRSL chronology and dust mass accumulation rates of the Nosak loess-palaeosol sequence in northeastern Serbia. Boreas 49, 841–857. https://doi.org/10.1111/bor.12459.
Perić, Z.M., Ryan, C., Alexanderson, H., Marković, S.B., 2024. Revised OSL chronology of the Kisiljevo loess-palaeosol sequence: new insight into the dust flux in the eastern Carpathian Basin during MIS 3 - MIS1. Quat. Int. https://doi.org/10.1016/j.quaint.2024.06.006.
Perić, Z.M., Ryan, C.S., Thompson, W., Radaković, M.G., Krsmanović, P., Alexanderson, H., Marković, S.B., 2025a. Palaeoenvironmental changes recorded at the velika vrbica loess-palaeosol sequence, wallachian Basin, during MIS 3–MIS 1. Boreas. https://doi.org/10.1111/bor.70009.
Perić, Z.M., Radaković, M.G., Marković, R.S., Marković, S.B., 2025b. A synthesis of luminescence and 14C dated dust mass accumulation rates for loess-palaeosol sequences from the middle danube basin. Boreas 54, 179–201. https://doi.org/10.1111/bor.12696.
Perić, Z.M., Stevens, T., Obreht, I., Hambach, U., Lehmkuhl, F., Marković, S.B., 2022b. Detailed luminescence dating of dust mass accumulation rates over the last two glacial-interglacial cycles from the Irig loess-palaeosol sequence, Carpathian Basin. Global Planet. Change 215, 103895. https://doi.org/10.1016/j.gloplacha.2022.103895.
Prescott, J.R., Hutton, J.T., 1994. Cosmic ray contributions to dose rates for luminescence and ESR dating: large depths and long-term time variations. Radiat. Meas. 23, 497–500. https://doi.org/10.1016/1350-4487(94)90086-8.

Sawakuchi, A.O., Jain, M., Mineli, T.D., Nogueira, L., Bertassoli, D.J., Häggi, C., Sawakuchi, H.O., Pupim, F.N., Grohmann, C.H., Chiessi, C.M., Zabel, M., Mulitza, S., Mazoca, C.E.M., Cunha, D.F., 2018. Luminescence of quartz and feldspar fingerprints provenance and correlates with the source area denudation in the amazon River basin. Earth Planet Sci. Lett. 492, 152–162. https://doi.org/10.1016/j.epsl.2018.04.006.

Schmidt, E.D., Machalett, B., Marković, S.B., Tsukamoto, S., Frechen, M., 2010. Luminescence chronology of the upper part of the Stari Slankamen loess sequence (Vojvodina, Serbia). Quat. Geochronol. 5, 137–142. https://doi.org/10.1016/J.QUAGEO.2009.09.006.

Stevens, T., Marković, S.B., Zech, M., Hambach, U., Sümegi, P., 2011. Dust deposition and climate in the carpathian basin over an independently dated last glacial-interglacial cycle. Quat. Sci. Rev. 30, 662–681. https://doi.org/10.1016/j.quascirev.2010.12.011.

Thiel, C., Buylaert, J.P., Murray, A., Terhorst, B., Hofer, I., Tsukamoto, S., Frechen, M., 2011. Luminescence dating of the Stratzing loess profile (Austria) - testing the potential of an elevated temperature post-IR IRSL protocol. Quat. Int. 234, 23–31. https://doi.org/10.1016/j.quaint.2010.05.018.

Tudyka, K., Koruszowic, M., Osadnik, R., Adamiec, G., Moska, P., Szymak, A., Bluszcz, A., Zhang, J., Kolb, T., Poręba, G., 2023. μRate: an online dose rate calculator for trapped charge dating. Archaeometry 65, 423–443. https://doi.org/10.1111/arcm.12828.

Wintle, A.G., Murray, A.S., 2006. A review of quartz optically stimulated luminescence characteristics and their relevance in single-aliquot regeneration dating protocols. Radiat. Meas. 41, 369–391. https://doi.org/10.1016/J.RADMEAS.2005.11.001.

Yi, S., Buylaert, J.P., Murray, A.S., Thiel, C., Zeng, L., Lu, H., 2015. High resolution OSL and post-IR IRSL dating of the last interglacial–glacial cycle at the Sanbahuo loess site (northeastern China). Quat. Geochronol. 30, 200–206. https://doi.org/10.1016/J.QUAGEO.2015.02.013.

Zhang, X.Y., Arimoto, R., An, Z.S., 1999. Glacial and interglacial patterns for Asian dust transport. Quat. Sci. Rev. 18, 811–819.

Zhao, H., Li, S.-H., 2005. Internal dose rate to K-feldspar grains from radioactive elements other than potassium. Radiat. Meas. 40, 84–93.